A&A 662, A40 (2022)
https://doi.org/10.1051/0004-6361/202243337

Astronomy & Astrophysics

The population of hot subdwarf stars studied with *Gaia*

IV. Catalogues of hot subluminous stars based on *Gaia* EDR3⋆

R. Culpan[1], S. Geier[1], N. Reindl[1], I. Pelisoli[2], N. Gentile Fusillo[3], and A. Vorontseva[4]

[1] Institut für Physik und Astronomie, Universität Potsdam, Haus 28, Karl-Liebknecht-Str. 24/25, 14476 Potsdam-Golm, Germany
e-mail: rick@culpan.de
[2] Department of Physics, University of Warwick, Coventry, CV4 7AL, UK
[3] European Southern Observatory, Karl Schwarzschild Straße 2, 85748 Garching, Germany
[4] Sixfold GmbH, Magirus-Deutz-Straße 16, 89077 Ulm, Germany

Received 16 February 2022 / Accepted 7 March 2022

ABSTRACT

In light of substantial new discoveries of hot subdwarfs by ongoing spectroscopic surveys and the availability of the *Gaia* mission Early Data Release 3 (EDR3), we compiled new releases of two catalogues of hot subluminous stars: The data release 3 (DR3) catalogue of the known hot subdwarf stars contains 6616 unique sources and provides multi-band photometry, and astrometry from *Gaia* EDR3 as well as classifications based on spectroscopy and colours. This is an increase of 742 objects over the DR2 catalogue. This new catalogue provides atmospheric parameters for 3087 stars and radial velocities for 2791 stars from the literature. In addition, we have updated the *Gaia* Data Release 2 (DR2) catalogue of hot subluminous stars using the improved accuracy of the *Gaia* EDR3 data set together with updated quality and selection criteria to produce the *Gaia* EDR3 catalogue of 61 585 hot subluminous stars, representing an increase of 21 785 objects. The improvements in *Gaia* EDR3 astrometry and photometry compared to *Gaia* DR2 have enabled us to define more sophisticated selection functions. In particular, we improved hot subluminous star detection in the crowded regions of the Galactic plane as well as in the direction of the Magellanic Clouds by including sources with close apparent neighbours but with flux levels that dominate the neighbourhood.

Key words. subdwarfs – Hertzsprung-Russell and C-M diagrams – binaries: general – stars: horizontal-branch – catalogs

1. Introduction

The name 'subdwarf' was suggested in 1939 by Kuiper et al. (1939) to describe the stars found between the main sequence and the white dwarf regions of the Hertzsprung-Russell diagram (HRD). Most of those cool objects of late spectral types were later identified as metal-poor main sequence stars from old Galactic populations. The first hot subdwarf stars with early spectral types were found somewhat later by Humason & Zwicky (1947) and in contrast to their cool siblings, their formation mechanism and evolutionary status are still unclear.

Many, but not all hot subdwarfs lie at the extreme blue end of the horizontal branch (extreme horizontal branch (EHB)) in the HRD (Heber 1986) (see Fig. 1). Only very few stars are predicted by single star evolution in this region as the evolutionary timescale of the post-asymptotic giant branch (post-AGB) phase is very short. Many hot subluminous stars are therefore likely to be helium-burning stars with longer evolutionary timescales. To evolve to the EHB, red giants or subgiants must lose almost their entire hydrogen envelope, which is explained by various scenarios of binary merger or mass transfer (Han et al. 2002, 2003). See Heber (2016) for a review. More recently, this region in the HRD was found to also contain cooling progenitors of helium white dwarfs (Heber et al. 2003) and other rare types of detached or accreting compact binary systems.

Initially, hot subdwarf stars were discovered via photometric surveys of faint blue stars (e.g. Humason & Zwicky 1947; Luyten & Miller 1951; Luyten 1953; Iriarte & Chavira 1957; Feige 1958; Chavira 1958, 1959; Haro & Luyten 1962; Slettebak & Brundage 1971; Berger & Fringant 1984; Green et al. 1986; Demers et al. 1986; Downes 1986). Kilkenny et al. (1988) published the first catalogue of 1225 spectroscopically identified hot subdwarf stars. See Lynas-Gray (2004) for a review of those early studies. Surveys mainly targeting extragalactic sources detected many more such stars (Hagen et al. 1995; Wisotzki et al. 1996; Stobie et al. 1997; Mickaelian et al. 2007; Mickaelian 2008) and Østensen (2006) compiled a database containing more than 2300 entries.

In the following decade, the Sloan Digital Sky Survey (SDSS) provided spectra of almost 2000 hot subdwarfs (Geier et al. 2015b; Kepler et al. 2015, 2016, 2019) and new samples of bright hot subdwarf stars were observed (Vennes et al. 2011). In parallel, more and more data from new large-area photometric and astrometric surveys were gathered in multiple bands from the ultraviolet to the far-infrared. The availability of this amount of high-quality data triggered the first data release of the catalogue of known hot subdwarf stars (Geier et al. 2017a).

In the following years, substantial new discoveries were made of hot subdwarfs and quantitative spectroscopic analyses of large samples have since been conducted in the course of ongoing spectroscopic surveys such as LAMOST (Lei et al. 2018, 2019, 2020; Luo et al. 2019, 2021) and SDSS (Geier et al. 2017b; Kepler et al. 2019). A major milestone was the publication of *Gaia* mission DR2 (Gaia Collaboration 2018), because

⋆ Catalogues are only available at the CDS via anonymous ftp to cdsarc.u-strasbg.fr (130.79.128.5) or via http://cdsarc.u-strasbg.fr/viz-bin/cat/J/A+A/662/A40

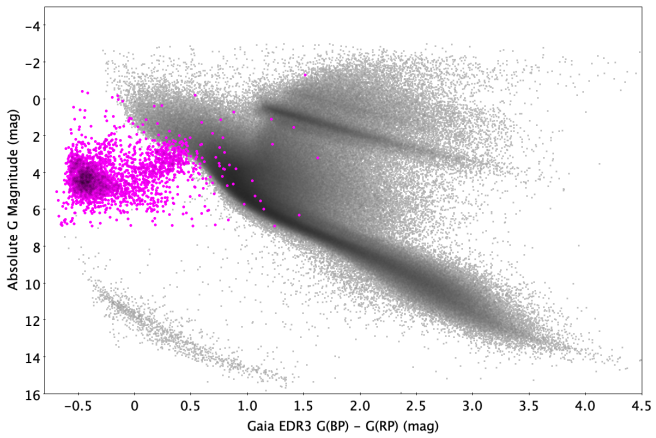

Fig. 1. Full-scale *Gaia* EDR3 colour–magnitude diagram (CMD) (grey dots) with the known hot subdwarfs from Geier (2020) (magenta circles) highlighting the *Gaia* EDR3 CMD region where hot subdwarfs are expected. Here we can see the EHB cluster of sources at $(G_{BP} - G_{RP}) \sim -0.35$, $G_{abs} \sim 4.5$ and the extended cloud of hot subdwarf plus main sequence binaries towards $(G_{BP} - G_{RP}) \sim 0.5$, $G_{abs} \sim 3.0$.

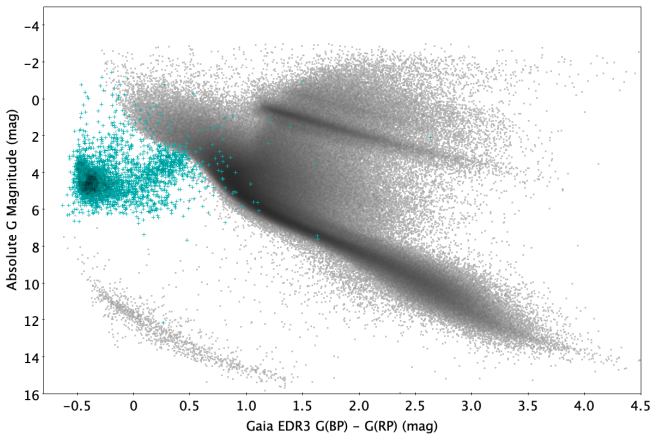

Fig. 2. Full-scale *Gaia* EDR3 colour–magnitude diagram (grey dots) with the known hot subdwarfs DR3 (cyan crosses). Due to the unreliable absolute G magnitudes of the remaining 2877 objects, only the 3373 objects from the DR3 catalogue of known hot subdwarfs that conform to the astrometric and photometric selection quality criteria (see Table 1.) are plotted. Here we can see the EHB cluster of sources at $(G_{BP} - G_{RP})$ −0.35, G_{abs} 4.5 and the extended cloud of hot subdwarf plus main sequence binaries towards $(G_{BP} - G_{RP})$ 0.5, G_{abs} 3.0.

it allowed us to use colour, absolute magnitude, and reduced proper motion criteria to identify 268 previously misclassified hot subdwarfs as white dwarfs, blue horizontal branch (BHB), and main sequence stars. The release of the second version of the catalogue (Geier 2020) contained 5874 unique sources, provided atmospheric parameters for 2187 stars, and radial velocities for 2790 stars from the literature. This added 528 newly discovered hot subdwarfs to the Geier et al. (2017a) catalogue (see Fig. 1).

The Geier et al. (2017a) catalogue has been used to determine selection criteria for an all-sky catalogue of hot subdwarf star candidates selected from *Gaia* DR2 (Gaia Collaboration 2018) by means of colour, absolute magnitude, and reduced proper motion cuts. This catalogue contains 39 800 unique sources, has a magnitude limit of $G < 19$ mag, and covers the whole sky with the exception of the Galactic plane and the direction of the Large and Small Magellanic Clouds (LMC/SMC). It should be fairly complete up to ∼1.5 kpc and the contamination by cooler stars should be about 10% (Geier et al. 2019).

Here we present new releases of the catalogue of known hot subdwarfs (DR3) and the catalogue of hot subluminous star candidates (DR2) based on improved data from *Gaia* EDR3 (Gaia Collaboration 2021a), new results from spectroscopic surveys, and an extensive literature search. The catalogue of known hot subdwarfs contains stars of spectral types O to B occupying the region in the colour–magnitude diagram between the more luminous main sequence stars of similar spectral type and the less luminous white dwarfs and their cooling curve. In addition, it also includes the known hot subdwarfs in binary systems with main sequence companions. The aggregated colour and absolute magnitude of these unresolved binaries is found between those of the individual stars causing the large spread seen in Fig. 1.

The *Gaia* EDR3 catalogue of hot subluminous stars contains candidates in the same region of the HRD. Next to single subdwarfs and composite subdwarf binaries, it also contains subluminous stars of A and early-F type.

The *Gaia* EDR3 hot subluminous star catalogue and the catalogue of known hot subdwarfs have been brought together to examine the possible effects of binarity on the *Gaia* EDR3 photometric and astrometric measurements and their associated errors. Differences have been found that correlate with the type of binary system that prevails.

The contents of this paper are as follows: Sect. 2 provides a catalogue of the known hot subdwarfs: Data Release 3. In Sect. 3 we describe how we constructed the hot subluminous star catalogue from *Gaia* EDR3. In Sect. 4 we consider astrometric and photometric indications of variability. Section 5 outlines the main specifications of the catalogues in terms of magnitude, distance and sky coverage. Section 6 contains a summary and the conclusions drawn.

2. Catalogue of known hot subdwarfs: Data Release 3

2.1. Input data

We complement the spectroscopically classified hot subdwarfs from the Geier (2020) catalogue with 224 newly discovered objects from DR6/7 of the LAMOST survey (Luo et al. 2021) (see Fig. 2). These latter authors also provide atmospheric parameters and radial velocities for more than 1500 hot subdwarfs observed in all the available releases of LAMOST. The second main source of new and refined classifications of 107 helium-rich hot subdwarf stars and related objects is provided by a targeted survey conducted with the South African Large Telescope (SALT) by Jeffery et al. (2021). The discovery of a large sample of eclipsing HW Vir type binaries with hot subdwarf primaries has been reported by Schaffenroth et al. (2019). Those that have been confirmed spectroscopically have been added to the catalogue. In contrast to the previous releases, we decided to also include the 196 spectroscopically identified hot subdwarfs in the globular clusters M80 (Moni Bidin et al. 2009), ω Cen (Moni Bidin et al. 2012; Latour et al. 2018b; Moni Bidin et al. 2009), and NGC 6752 (Heber & Kudritzki 1986; Moni Bidin et al. 2007).

A further extension of our catalogue is provided by the rare spectroscopically identified stars in the post-AGB region and central stars of planetary nebulae (CSPNe), which are situated below the MS and have not yet evolved to the WD stage. Thus, they also belong to the population of the hot subdwarfs. The spectroscopically identified CSPNe are compiled in the catalogue of Weidmann et al. (2020). From this sample, we

selected CSPNe with classifications as O-type or emission line stars excluding both hot WDs and CSPNe located on or above the MS in the CMD. Those are regarded as the best candidates for hot subluminous stars, but as no clear distinction is possible, the catalogue of Weidmann et al. (2020) should be regarded as complimentary to our catalogue.

Adding the known post-AGB stars without nebulae, we find a total of 402 such objects in the literature (Rauch & Werner 1995; Dreizler 1998; Napiwotzki 1999; Werner et al. 2004a,b, 2005, 2014; Herald & Bianchi 2011; Ziegler 2012; Reindl et al. 2014, 2016, 2017, 2020; Aller et al. 2015; de Marco et al. 2015; Werner & Rauch 2015; Hillwig et al. 2017; Löbling 2020). The catalogue now includes, for the first time, all spectroscopically confirmed hot subdwarf stars regardless of their Galactic population and their evolutionary stage.

In addition, several recent studies reported the discovery of individual subdwarfs (Hillwig et al. 2017; Kupfer et al. 2017a,b, 2020, 2022; Holdsworth et al. 2017; Ratzloff et al. 2019, 2020; Kilkenny et al. 2019; Bell et al. 2019; Hogg et al. 2020; Silvotti et al. 2021; Pelisoli et al. 2021; Vos et al 2021; Dorsch et al. 2022; Silvotti et al. 2022; Werner et al. 2022a,b), all of which are included in our compilation.

2.2. Astrometry and multi-band photometry

Gaia EDR3 (Gaia Collaboration 2021a) astrometry and photometry has been added to the catalogue. The zero-points of the parallax measurements have been corrected as described in Lindegren et al. (2021b) and the corrected *Gaia* parallaxes are provided in addition to the uncorrected ones.

The sources for the further multi-band photometry as well as the Galactic extinction and reddening provided in the catalogue are described in Geier (2020). Only the infrared photometry in the $YJHK$ bands from the Visible and Infrared Survey Telescope for Astronomy (VISTA) Hemisphere Survey has been updated to the most recent DR5 (McMahon et al. 2013).

2.3. Cleaning the catalogue

To remove misclassified objects, we used colour indices as described in Geier (2020). As most of the newly discovered subdwarfs have been well classified and analysed, we did not find any cool outliers in this data release. Due to the PNs surrounding them and the fact that many of them are found at low latitudes and high reddening, we did not apply any colour cleaning to the CSPNe. Calculating the absolute magnitudes of all stars with accurate parallaxes (parallax error smaller than 20% and zero-point correction applied), we identified several misclassified white dwarfs (WDs) with $M_G < 6.5$ mag and also brighter objects such as main sequence B (MS-B) stars. The reduced proper motion $H = G + 5\log\mu + 5$ was calculated for stars with parallax errors ≥20% using the *Gaia* G magnitudes and proper motion (μ) to identify additional WDs with $H > 15$. However, we find no additional misclassified objects.

Several misclassified subdwarfs were found by cross-matching our sample with the SIMBAD database, the most recent analysis of the MMT hypervelocity star survey (Brown et al. 2014; Kreuzer 2021), and the list of misclassified hot subdwarfs from the LAMOST survey (Luo et al. 2021). The main contaminants of our sample are WDs and MS-A/B-type stars as well as a few cataclysmic variables. However, a galaxy and an active galactic nucleus were also previously classified as hot subdwarfs.

The 182 misclassified objects are provided with their correct classifications as a separate catalogue. Based on their previous classifications as sdBs or sdOs and their colours, a tentative classification of the WD candidates as either DAB (hydrogen and neutral helium lines) or DAO (hydrogen and/or ionised helium lines) candidates is provided. In the absence of a previous detailed classification, they are classified as WD. The final DR3 catalogue of known hot subdwarfs contains 6616 unique objects. The predominance of hot subdwarfs outside the Galactic plane (see Fig. 3) is due to observational limitations in crowded regions. For a description of the catalogue columns of both the DR3 catalogue and the catalogue of misclassified objects, see Table A.1.

2.4. Classification, spectroscopic parameters, and radial velocities

For the spectroscopic and photometric classifications, we follow the scheme outlined in Geier et al. (2017a) and updated in Geier (2020). To complement the spectroscopic classes sdB, He-sdB, sdOB, He-sdOB, sdO, and He-sdO, we introduce the additional classes O(H), O(He), PG1159, and [WR] to classify the hotter central stars of planetary nebulae (CSPNe) and other post-AGB stars in our sample. O(H) stars have hydrogen-rich spectra similar to sdOs with Balmer lines and usually only one He II line at 4686 Å. O(He) stars exclusively show He II and some weaker metal lines of high ionization stages, while PG1159 stars show strong carbon lines in addition to the He II lines in the optical. [WR] stars are hot and luminous CSPNe with spectra dominated by emission lines.

The catalogue contains spectroscopic parameters such as effective temperatures, surface gravities, and helium abundances. In this catalogue, we aim to provide those parameters for all the stars where such data are provided in the literature. To achieve that in the most efficient way, we started with papers containing parameters of larger samples of hot subdwarfs. For all the remaining stars in the catalogue, we queried the available literature using the SIMBAD database and collected the atmospheric parameters. For the CSPNs, we only include atmospheric parameters determined with non-local thermodynamic equilibrium (NLTE) models, which we consider as reliable (for the references from the literature see Table A.1).

As the main purpose of this catalogue is the identification and classification of hot subdwarf stars, only one set of atmospheric parameters is provided for each star, even if several different values are provided in the literature. In total, 3087 objects in our catalogue have measured atmospheric parameters taken from the literature. This is, again, a significant increase with respect to the 2187 objects included in Geier (2020) and should now be close to complete, especially regarding results taken from older literature.

Radial velocities (RVs) are provided for the 2791 stars with spectra in the SDSS and LAMOST data archives. However, for the most helium-rich objects, systematic offsets by up to $\sim$100 km s^{-1} are possible owing to cross-correlation with inadequate template spectra (Geier et al. 2015a, 2017a). If available, we used the RVs provided by Luo et al. (2021) for the LAMOST spectra, because they were measured using appropriate models and should not be affected by such systematic errors.

3. Constructing the hot subluminous star catalogue from *Gaia* EDR3

The aim of the European Space Agency's *Gaia* mission was to create a three-dimensional map of our Galaxy. *Gaia* Early Data

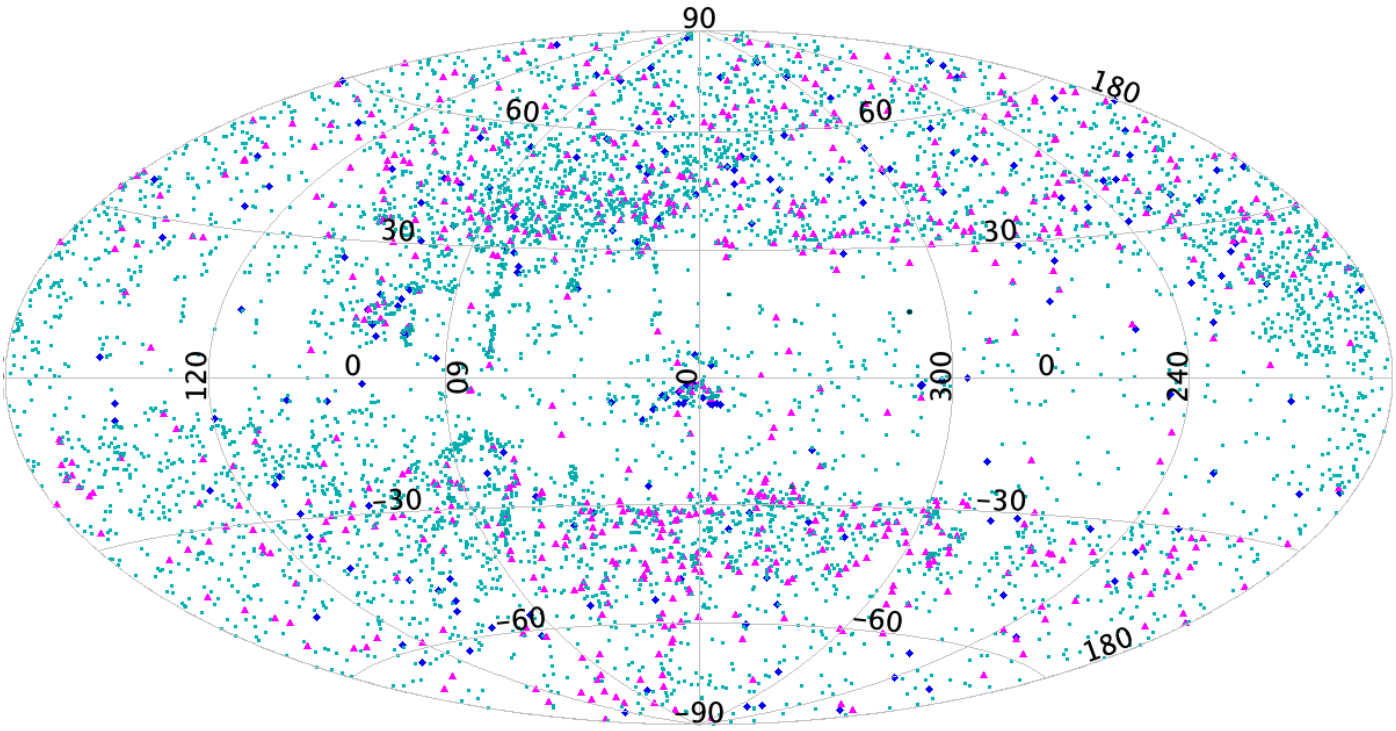

Fig. 3. Full-sky distribution of known hot subdwarfs DR3: Known hot subdwarfs with no binarity observed (cyan squares), known hot subdwarfs in wide binary systems (magenta triangles), and known hot subdwarfs in close binary systems with WD, dwarf-M type, or brown dwarf companions (blue diamonds).

Release 3 (EDR3; Gaia Collaboration 2021b) has charted over 1.8 billion sources and contains astrometry and photometry data acquired during the first 34 operational months. The procedure we used to generate our catalogue is based on that used in Geier et al. (2019) but modified to reflect the differences between the *Gaia* DR2 and EDR3 data sets in accordance with the recommendations made by Fabricius et al. (2020) that the *Gaia* EDR3 data set be considered independently of DR2. As such, we did not directly use any of the results from Geier et al. (2019). Furthermore, given the proven high quality of the *Gaia* data, we decided to compile the catalogue from these data only and not include ground-based datasets as in Geier et al. (2019).

3.1. Hot subluminous star selection using parallax measurements

We selected all *Gaia* EDR3 objects with good parallax measurements (`parallax_over_error` > 5; `parallax` > 0), and used the colour criteria ($-0.7 < (G_{\rm BP} - G_{\rm RP}) < 0.7$) and the absolute magnitude criteria ($-5 < G_{\rm abs} < 7$). The absolute G magnitude was calculated using:

$$\texttt{abs\_g\_mag} = \texttt{phot\_g\_mean\_mag} + 5 + 5\log_{10}(\texttt{parallax}/1000). \quad (1)$$

Applying these criteria resulted in 3 213 406 objects from the *Gaia* EDR3 catalogue. The criteria used were less restrictive than the ($-1 < G_{\rm abs} < 7$; $-0.7 < (G_{\rm BP} - G_{\rm RP}) < 0.7$) used for the Geier et al. (2019) catalogue. This was done to ensure that all possible hot subluminous stars were considered. Visual comparison of the respective CMDs showed this to be the case.

We calculated the corrected BP and RP flux excess factor (`phot_bp_rp_excess_factor_corrected`) using the equations found in Sect. 6 of Riello et al. (2021) and applied the following photometric and astrometric quality criteria: `astrometric_sigma5d_max` < 1.5 limiting the five-dimensional uncertainty in the astrometric solution (Lindegren et al. 2018, 2021a); |`phot_bp_rp_excess_factor_corrected`| < 0.6 to act as a filter to remove sources with inconsistencies in G, $G_{\rm BP}$, and $G_{\rm RP}$ photometry (Riello et al. 2021). Application of these quality criteria reduced the number of potential candidates with good parallax to 3 195 369.

The correction for parallax bias with regard to magnitude (zero point correction - zpc) outlined in Lindegren et al. (2021b) was not taken into account for the candidate selection as many of the hot subluminous stars lie in a parameter range where the correction is not well defined. To maintain internal consistency without unnecessarily removing objects without a well-defined zero-point we have opted to use *Gaia* EDR3 parallax without bias correction.

It should be noted that the astrometric quality criteria from Lindegren et al. (2018, 2021a) based on the renormalised unit weight error (`ruwe`) and astrometric excess noise significance (`astrometric_excess_noise_sig`) were not used as they are sensitive to astrometric binaries with unresolved companions and we do not aim to exclude such systems.

We created a cut in *Gaia* EDR3 colour and absolute magnitude parameter space by dividing the *Gaia* EDR3 hot subdwarf CMD parameter space into a 100×100 grid and counting the number of objects in each subregion. We generated a polynomial in colour–magnitude space (see Table 1) to follow the trough in values between the hot subdwarf and main sequence clusters of objects and act as a main sequence region rejection criterion (see the cyan line in Fig. 4).

Applying the selection criteria for sources with a parallax error of less than 20% (criteria 1, 2, 3, and 4; see Table 1)

Table 1. Selection criteria applied to *Gaia* EDR3 to define the hot subluminous star candidate selection from colour and absolute G magnitude using sources with good parallax.

1. *Gaia* EDR3 initial hot subluminous star CMD ranges $-0.7 \leq (G_{BP} - G_{RP}) \leq 0.7$ $-5 \leq G_{abs} \leq 7$
2. Astrometric quality selection criteria `parallax` > 0 `parallax_over_error` > 5 `astrometric_sigma5d_max` < 1.5
3. Photometric quality selection criteria |`phot_bp_rp_excess_factor_corrected`| < 0.6
4. *Gaia* EDR3 CMD main sequence region rejection criterion $G_{abs} < 17.7(G_{BP} - G_{RP})^3 - 6.9(G_{BP} - G_{RP})^2 + 7.35(G_{BP} - G_{RP}) + 1.95$
5. Strict hot subluminous star selection criterion $G_{abs} < 12.0(G_{BP} - G_{RP})^3 + 12.9(G_{BP} - G_{RP})^2 + 6.8(G_{BP} - G_{RP}) + 3.53$

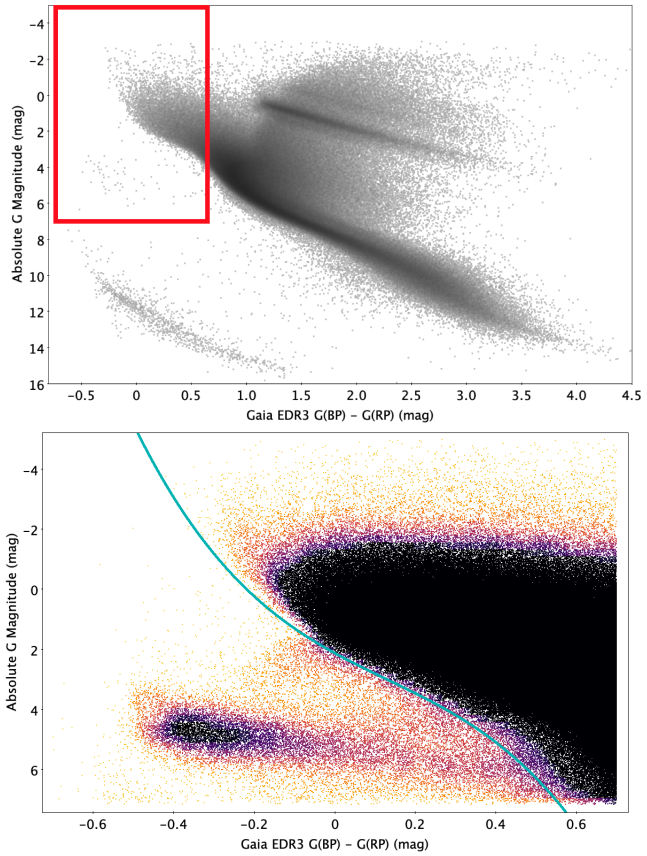

Fig. 4. *Gaia* EDR3 Colour magnitude diagram (CMD). *Upper panel*: full-scale *Gaia* EDR3 CMD (grey dots) with the *Gaia* EDR3 initial hot subluminous star CMD range (red rectangle) used in subsequent CMD plots; *lower panel Gaia* EDR3 initial hot subluminous star CMD region. The colour scale shows the number density of objects. The cyan line shows the cutoff used to remove the main sequence region.

reduced the number of potential hot subluminous stars to 16 959 objects.

It is known that sources in regions of high apparent stellar density are prone to inaccurate astrometry. When these inaccurate measurements are repeatable, the astrometric quality criteria will not flag such measurements as being erroneous (Gentile Fusillo et al. 2019, 2021; Geier et al. 2019; Pelisoli & Vos 2019; Culpan et al. 2021). Furthermore, regions of high apparent stellar density are also known to be more susceptible to inaccuracies in the determination of the G_{BP} and G_{RP} background as well as blending effects (Riello et al. 2021).

In order to minimise these crowded region effects, we defined the subset of objects in the *Gaia* EDR3 CMD hot subluminous star region with no apparent neighbours within a 5 arcsec radius. We find 10 672 such candidates and refer to them here as the Parallax Selection 1 set. We next considered those objects with one or more apparent neighbours within 5 arcsec. The total G flux from the hot subluminous star and the apparent neighbours within 5 arcsec was calculated. Next we selected the hot subluminous stars whose G flux dominated the 5 arcsec neighbourhood flux. The criterion for this was at least 70% of the 5 arcsec neighbourhood G band flux coming was from the hot subluminous star itself. There are 1147 such candidates, which we refer to as the Parallax Selection 2 set.

Finally, we considered the remaining candidate objects whose G flux was less than 70% of the total 5 arcsec neighbourhood G flux. As both the astrometry and photometry might be adversely affected for these objects, we applied a stricter parallax quality criterion (parallax error <10%) and a stricter cutoff (see criterion 5 in Table 1) to ensure that only the objects whose colour lies directly within the most populated region of the hot subluminous star CMD cloud were selected. It was considered highly unlikely that objects that were bluer than a hot subdwarf were then reddened by extinction to make them lie in this region. We generated a polynomial for the strict hot subdwarf selection criterion (see Fig. 5 bottom left panel). There are 1304 candidate objects in this final Parallax Selection 3 set.

The three parallax selection sets identified here (see Fig. 5) resulted in 13 123 hot subluminous stars (Final Parallax Selection) selected using colour and absolute G magnitude. A summary of the selection criteria used and their effect on the number of candidate objects found in the *Gaia* EDR3 hot subluminous star catalogue can be seen in Table 3.

3.2. Hot subluminous star parameter determination for candidate selection using proper motion measurements

The use of reduced proper motion as a proxy for absolute G magnitude when identifying hot subluminous stars, white dwarfs, and BHB objects has become common practice, and was used by Gentile Fusillo et al. (2021), Geier et al. (2019), and Culpan et al. (2021).

Using parallax errors <20% as a selection criterion effectively limits the distance at which we are able to select hot subluminous stars. Around 90% of the Final Parallax Selection is found at distances of less than 3 kpc from the Sun. By using reduced proper motion as a proxy for absolute G magnitude, we are able to benefit from the fact that there are many objects in the *Gaia* EDR3 data set that have a parallax error >20% yet still have reliable proper motion measurements.

Plotting the Final Parallax Selection objects in colour reduced proper motion space (see Fig. 6 upper panel) we were able to find the parameter space where we could expect to discover more distant candidate objects. In order to do this, the `reduced_proper_motion` (H_G) and the `proper_motion_over_error` ($\mathtt{pm}/\sigma_{pm}$) were calculated for all 3 213 406 objects in the *Gaia* EDR3 hot subluminous star CMD range where:

$$H_G = G + 5\log_{10}(\mu) + 5 \quad (2)$$

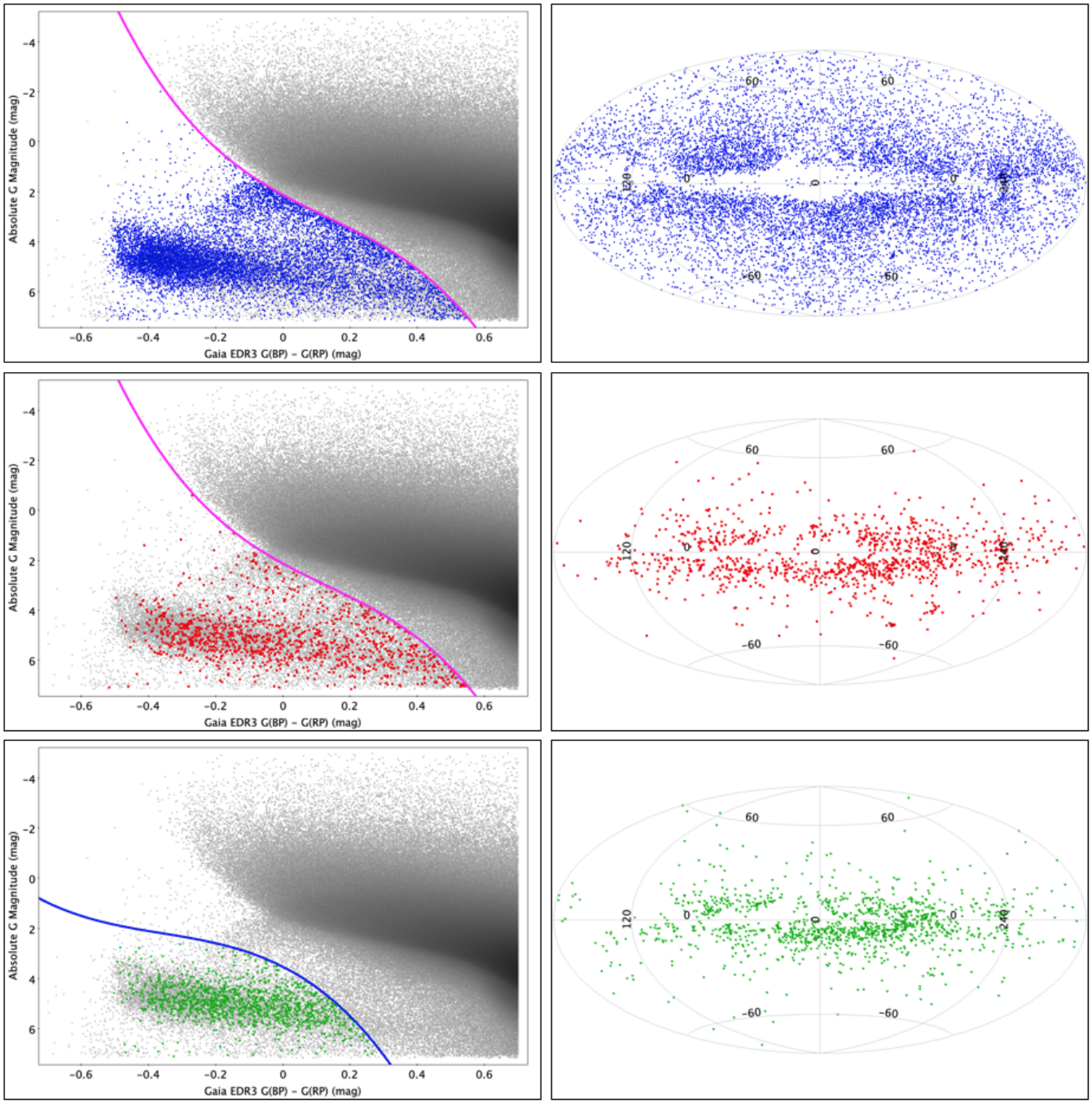

Fig. 5. *Left column*: *Gaia* EDR3 colour–magnitude diagrams showing the 3 213 406 initial candidate objects (grey dots) with the *Gaia* EDR3 CMD hot subluminous star region selection criteria (magenta line - *top and middle rows*) and the strict hot subluminous star-selection criterion (blue line - *bottom row*) (see Table 1). *Right column*: sky distribution of the parallax selection candidate objects. *Top row*: parallax Selection 1 objects (blue circles). *Middle row*: parallax Selection 2 objects (red squares). *Bottom row*: parallax Selection 3 objects (green triangles).

$$\sigma_{\rm pm} = \frac{\sqrt{(\sigma_{\rm pmra}\texttt{pmra})^2 + (\sigma_{\rm pmdec}\texttt{pmdec})^2}}{\rm pm}. \quad (3)$$

The plot of colour versus reduced proper motion for the 3 213 406 initial selection and the Final Parallax Selection superimposed (see Fig. 6, upper panel) shows, as expected, the same general form as the colour–magnitude plot (lower panel), but with the hot subluminous star region less well separated from the main sequence region. This gave us confidence that using reduced proper motion as a proxy for absolute magnitude is a valid method for this data set albeit with lower completeness and higher levels of contamination than found in the Final Parallax Selection. A discussion of the relative contamination and completeness between the Final Parallax Selection and the Proper Motion Selection can be found in Sect. 5.

As was done in the parallax selection procedure, a polynomial line was defined to separate the cloud of hot subluminous stars and the main sequence objects. For the reduced proper motion selection, this was done iteratively by comparing the results for the same objects in the colour versus reduced proper motion (colour-$H_{\rm G}$) diagram (see Fig. 6 upper panel) and the CMD (see Fig. 6 lower panel).

Table 2. Selection criteria applied to *Gaia* EDR3 to define the hot subdwarf candidate selection from colour and reduced proper motion using sources with unreliable parallax measurements.

1. *Gaia* EDR3 hot subluminous star colour-H_G ranges
$-0.7 \leq (G_{BP} - G_{RP}) \leq 0.7$
$-10 \leq H \leq 17$
2. Astrometric quality selection criteria
`parallax_over_error` ≤ 5
`pm_over_error` > 5
`astrometric_sigma5d_max` < 1.5
3. Photometric quality selection criteria
(`phot_bp_n_obs` > 2 AND `phot_rp_n_obs` > 2) OR `phot_g_mean_mag` < 19
4. *Gaia* EDR3 colour-H_G main sequence region rejection criterion
$H < -9.26(G_{BP} - G_{RP})^2 + 24.4(G_{BP} - G_{RP}) + 10.8$
5. White dwarf region rejection criterion
$H < 342.5(G_{BP} - G_{RP})^4 + 40.8(G_{BP} - G_{RP})^3 + 13.7(G_{BP} - G_{RP})^2 + 4.6(G_{BP} - G_{RP}) + 14.7$
6. Magellanic Cloud rejection criteria
within 15° of RA = 81.28°, Dec = −69.78° OR within 9° of RA = 12.8°, Dec = −73.15°

3.3. Reduced proper motion hot subdwarf candidate selection

We found 7 390 541 objects within the hot subluminous star colour–H_G region given in Sect. 3.3 (see Table 2). The use of proper motion (`pm`) in calculating reduced proper motion is directly analogous to the use of parallax in calculating absolute magnitude. Thus, an equivalent quality criterion of proper motion error <20% was applied (Gentile Fusillo et al. 2021; Culpan et al. 2021). This reduces the dataset to 6 860 074 objects.

Comparison of the colour–H_G plot for the parallax error <20% objects (see Fig. 6 upper panel) and the parallax error ≥20% objects (see Fig. 7) showed that a very different population of stars is present in the parallax error ≥20% selection. Using a parallax error <20% cutoff criterion is, as stated in Sect. 3.2, effectively limiting the distance of the selected objects to 2–3 kpc from the Sun. Considering objects at greater distances brings with it considerable contamination from the Magellanic Clouds. The region around the Magellanic Clouds was therefore removed, reducing further the number of objects to 4 856 823. Applying the astrometric and photometric quality criteria and the *Gaia* EDR3 colour–H_G diagram main sequence region rejection criterion that was found in Sect. 3.2 (see Table 2) to the remaining sources leaves 92,409 hot subluminous candidates.

We then applied the same filtering criteria for crowded region effects as used in the Parallax Selection 1 and Parallax Selection 2, resulting in 66 393 objects with no apparent neighbours within 5 arcsec (Proper Motion Selection 1) and 7044 objects where at least 70% of the total flux from within a 5 arcsec radius came from the candidate object (Proper Motion Selection 2).

3.4. Proper motion selection: white dwarf contamination

We saw a cloud of objects that were present at high reduced proper motions (see Fig. 7). These were not seen in the Final Parallax Selection (see Fig. 6 upper panel). We made a colour–H_G plot with the number density plotted on the colour axis using the same method as outlined in Sect. 3.1 and observed two clear

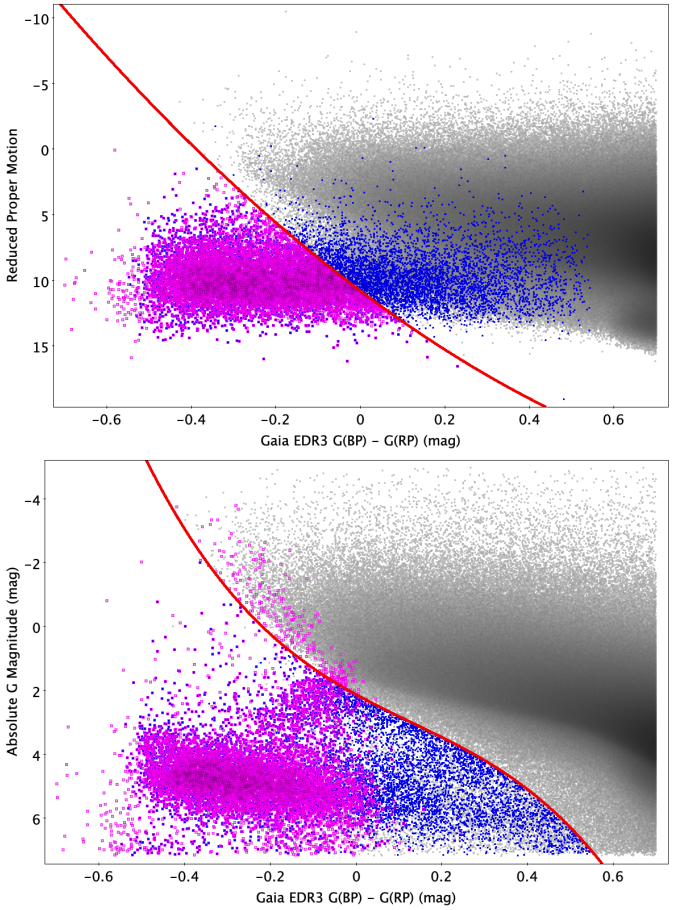

Fig. 6. *Upper panel*: *Gaia* EDR3 colour-reduced proper motion diagram. *Lower panel*: *Gaia* EDR3 colour–magnitude diagram. Both showing the initial parallax selection (grey dots) and Final Parallax Selection (blue circles) and reduced proper motion selection (magenta squares). The polynomial lines are defined as the cutoff criteria to remove the main sequence objects in colour-reduced-proper-motion space and colour–magnitude space, respectively.

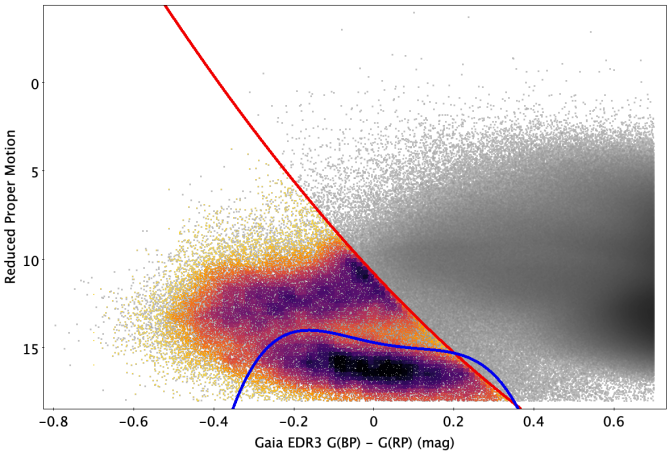

Fig. 7. *Gaia* EDR3 colour-reduced proper motion diagram for the hot subluminous star region. The grey dots show the objects outside the Magellanic Clouds that conform with all quality criteria. The colour scale shows the number density of Proper Motion Selection 1 and 2 objects in colour–H_G space. The red line shows the cutoff used to remove the main sequence region. The blue line shows the cutoff used to remove the white dwarf region.

concentrations of objects in colour–H_G space. Overlaying the high-probability white dwarf candidates in the reduced proper motion extension from Gentile Fusillo et al. (2021) shows that the cloud at higher reduced proper motions is white dwarf contamination. An additional cutoff was therefore made to reduce this white dwarf contamination (see Fig. 7). Applying the white-dwarf-rejection criterion leaves 48 462 hot subluminous star candidates (Final Proper Motion Selection). For a summary of the selection criteria and their effects on the number of candidate objects, see again Table 3.

4. Indications of variability

The formation and evolution of hot subdwarf stars is still not fully understood but mass loss and mass transfer with binary partners is thought to play a major role (Geier et al. 2017a; Pelisoli et al. 2020). We examined both the astrometric and photometric variability using different methods when applied to the *Gaia* EDR3 hot subluminous star catalogue and the known hot subdwarf catalogue and compared the results.

Astrometric variability, where the centre of an object moves between different images, is a known method to detect stellar companions (Lindegren et al. 2018, 2021a; Belokurov et al. 2020; Penoyre et al. 2021). The use of photometry to detect variability faces additional challenges as the uncertainty in the mean flux published in *Gaia* EDR3 is the standard deviation of the flux measurements with a weighting factor applied. However, this weighting factor is not provided. Many of the published methods (Chornay et al. 2021; Mowlavi et al. 2021) assume that the weighting factors are equal. The errors in the photometric noise are not only dependent on the variability of a candidate object, but also on colour, magnitude, sky background, and stray light. Different apparent magnitudes also have different acquisition and calibration parameters. Despite these limitations, the consideration of sources with anomalous flux error has led to successful identification of variable objects (Gentile Fusillo et al. 2021; Chornay et al. 2021; Mowlavi et al. 2021; Guidry et al. 2021).

4.1. Photometric variability

To investigate the photometric variability, we applied the methods described in Gentile Fusillo et al. (2021) and Guidry et al. (2021) and compared the results. Both of these methods were developed to identify photometric variability in white dwarfs which are close neighbours to hot subdwarfs in the Hertzsprung-Russell diagram. As such we considered it likely that these methods could be applied to hot subdwarfs.

The excess flux error method presented in Gentile Fusillo et al. (2021) compares the `phot_g_flux_error` of each candidate object to the median G flux error of 500 similar objects in terms of colour (`bp_rp`), G flux ($\log_{10}$ `phot_g_mean_flux`), and the number of observations (`phot_g_n_obs`) taken from the full *Gaia* EDR3 catalogue. A more precise description of the method and the evaluation can be found in Gentile Fusillo et al. (2021). This method, when applied to the Final Parallax Selection, found that 9.6% (1308 of 13 123) of the candidate objects with a parallax error <20% showed an excess of flux error indicating variability (see Fig. 8).

This method was also applied to the catalogue of known hot subdwarfs. We found that 7.6% of hot subdwarfs in wide binary systems and 23% of hot subdwarfs in close binary systems (see Fig. 9) showed an excess in flux error. Also, 5.2% of hot subdwarfs with no indication of binarity display an excess in flux error.

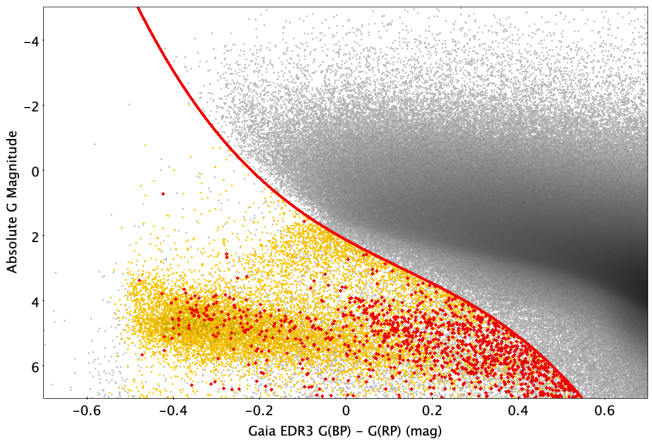

Fig. 8. *Gaia* EDR3 colour–magnitude diagram for the hot subluminous star region showing the initial parallax selection (grey dots), Final Parallax Selection (yellow circles), and hot subluminous stars found to have an excess flux error that indicates variability. The red line shows the cutoff used to remove the main sequence region.

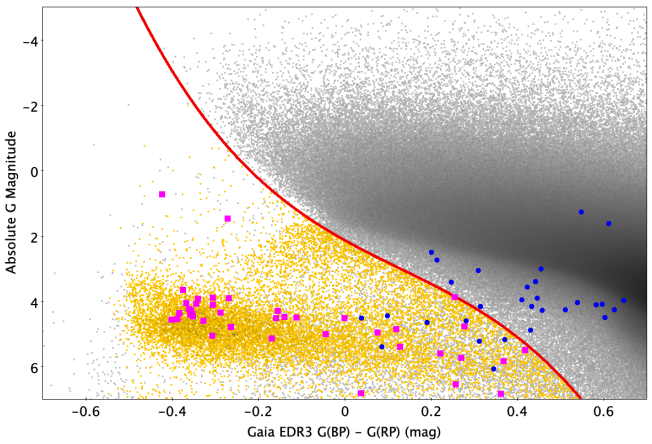

Fig. 9. *Gaia* EDR3 colour–magnitude diagram for the hot subluminous star region showing the initial parallax selection (grey dots), Final Parallax Selection (yellow circles), known hot subdwarfs in wide binary systems displaying an excess in flux error (blue circles), and known hot subdwarfs in close binary systems that display an excess in flux error (magenta squares). The red lines show the variability cutoffs used.

The results show a higher incidence of variability in composite systems when compared to single star systems. This might be due to intrinsic variability of the cool main sequence companions, which tend to show variations caused by rotation and spots (Pelisoli et al. 2020). The percentages found also show that close binary systems are more likely to exhibit photometric variability that is detectable with this method than wide binary systems. This is unsurprising as the amplitude of photometric variations is larger in close binary systems when compared to wider binaries with main sequence companions. Furthermore, there is a significant fraction of close binary systems that show eclipses, reflection effects or ellipsoidal variations among the hot subdwarf population (e.g. Schaffenroth et al. 2019; Pelisoli et al. 2021).

The method to detect variability that was proposed by Guidry et al. (2021) calculates a *Gaia* variability metric using *Gaia* photometry (*G* flux error, apparent *G* magnitude, *G* flux, and the number of observations) and a Zwicky variability metric using photometry data from the Zwicky Transient Facility. This method is calibrated to white dwarfs.

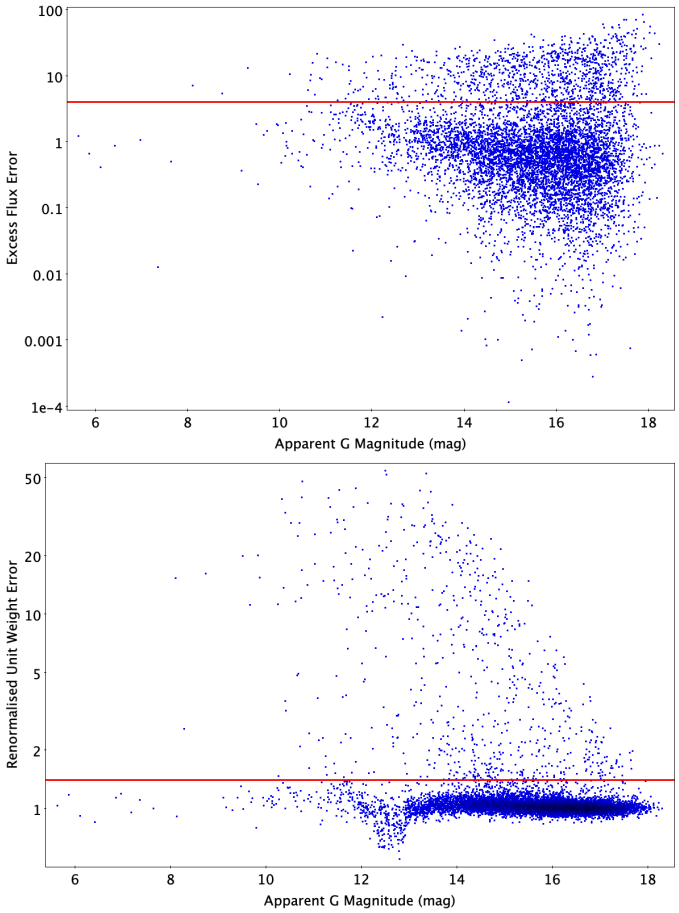

Fig. 10. Astrometric and photometric fluctuation indicators versus absolute G magnitude. *Upper panel*: distribution of excess flux error versus apparent G magnitude for all sources in the final parallax selection. The horizontal red line shows the cutoff used as the limit for variability detection. *Lower panel*: distribution of re-normalised unit weight error versus apparent G magnitude for all sources in the final parallax selection. The horizontal red line shows the cutoff used as the limit for variability detection.

The *Gaia* variability metric, when used alone, was found to be less effective than the excess flux error method for our data set. We considered this to be due to the fact that this was only one part of the full method and did not include colour as a comparison criterion. Comparing the results of the two methods revealed an unwanted colour dependency in the levels of variability found using the *Gaia* variability index from Guidry et al. (2021).

4.2. Astrometric variability

We used the *Gaia* EDR3 output renormalised unit weight error (`ruwe`) (Lindegren et al. 2018, 2021a) – a dimensionless measure of how much the centre of an object moves between different images – as an indicator for possible binarity. Identifying binarity from astrometric variability is currently planned for *Gaia* Data Release 3. Plotting `ruwe` versus the excess flux error (see Fig. 11) shows that there is a correlation between photometric and astrometric error excesses. Taking `flux_error_excess` > 4 (Gentile Fusillo et al. 2021) (see Fig. 10 upper panel) and `ruwe` > 1.4 (see Fig. 10 lower panel) as the regions where variability has been detected, we see that known hot subdwarfs in wide binary systems display excess errors in both the astrometric and photometric domains. Hot subdwarfs with close binary partners display only photometric error excesses.

As the known composite hot subdwarf binaries with solved orbits have periods of the order of years (e.g. Vos et al 2018), they should also be detectable by *Gaia* astrometry due to the comparable duration of the *Gaia* mission. It is therefore not surprising that many of them show astrometric excesses in addition to the photometric variability discussed in the previous section. The known hot subdwarfs in close binary systems have orbital periods of the order of hours to days (e.g. Kupfer et al. 2015) and are not expected to show astrometric variability.

5. Completeness and contamination

To estimate the completeness and contamination level of the *Gaia* EDR3 catalogue of hot subluminous stars, we made some comparisons within the catalogue itself and also with the catalogue of known hot subdwarfs.

5.1. Parallax versus proper motion selection

When considering all objects with a parallax error ≤20% we find 8694 of the 13 123 objects in the Final Parallax Selection are also selected using the proper motion selection criteria. This gives us a 66% completeness of the proper motion selection compared to the parallax selection.

There is a strong colour dependence in the completeness of the proper motion selection versus the parallax selection (see Fig. 6 lower panel). The reduced proper motion selection criteria find nearly all of the Final Parallax selection in the range $-0.7 < G_{\rm BP} - G_{\rm RP} < -0.15$ but find virtually no redder objects where $G_{\rm BP} - G_{\rm RP} \geq -0.15$.

Furthermore, we find only 10 512 parallax error ≤20% objects were selected using the proper motion criteria of which 2967 were not in the Final Parallax Selection. This gives a 28% contamination of the proper motion selection compared to the parallax selection.

The peak in the distance histogram (see Fig. 14) at 1.8 kpc indicates that the Final Parallax Selection is reasonably complete out to this distance for those hot subdwarfs that are not in binary systems or have unseen binary companions. When we make the approximation that all hot subdwarfs have an absolute magnitude of 4.5, then we can calculate an approximate distance to the objects selected according to their reduced proper motion using:

$$d \approx 10^{(0.2(\texttt{phot\_g\_mean\_mag}-4.5+5))}. \quad (4)$$

Using this equation, we find that the distance distribution of the Final Proper Motion Selection (see Fig. 15) peaks at ∼4 kpc with candidates found out to ∼9 kpc.

5.2. Known hot subdwarf and Gaia EDR3 subluminous star catalogue comparison

We find 3847 of the known hot subdwarfs to have a parallax error of <20%, of which 3246 (84%) are found within the Final Parallax Selection. As can be seen in Fig. 12, the majority of the known hot subdwarfs that are not in the Final Parallax Selection are those in binary systems with main sequence companions which, due to their redder composite colour, are located beyond our colour cut.

Of the remaining 2759 known hot subdwarfs that do not have a parallax error of <20%, we find 1715 (62%) in the Final Proper Motion Selection (see Fig. 13). In total, 5562 (84%) of the 6616 known hot subdwarfs are also present in the *Gaia* EDR3 hot subluminous star catalogue.

Table 3. Effect of the hot subluminous star selection criteria for the parallax selection and the proper motion selection as outlined in Sect. 3.

Selection criteria	Object count
Parallax selection criteria:	
1. Parallax >0, parallax error <20%, initial hot subdwarf CMD ranges	3 213 406
2. Position 1 + astrometric quality criteria	3 213 398
3. Position 2 + photometric quality criterion	3 195 369
4. Position 3 + CMD main sequence rejection criterion	16 959
5a. Position 4 + no apparent neighbours within 5 arcsec	10 672
5b. Position 4 + faint apparent neighbours within 5 arcsec	1147
5c. Position 4 + bright apparent neighbours within 5 arcsec + strict hot subdwarf cutoff	1304
6. Final parallax selection 5a + 5b + 5c	13 123
Proper Motion Selection Criteria	
7. Hot subdwarf colour-H_G range, parallax error ≥20%	7 390 541
8. Position 7 + proper motion error <20%	6 860 074
9. Position 8 + removal of the Magellanic Clouds direction	4 856 823
10. Position 9 + astrometric and photometric quality criteria	4 784 233
11. Position 10 + colour-H_G main sequence rejection criterion	92 409
12a. Position 11 + no apparent neighbours within 5 arcsec	66 393
12b. Position 11 + faint apparent neighbours within 5 arcsec	7044
13. Positions 12a+12b + white dwarf rejection criterion	48 462

Notes. The definition of 'bright' and 'faint' apparent neighbours is described in Sect. 3.

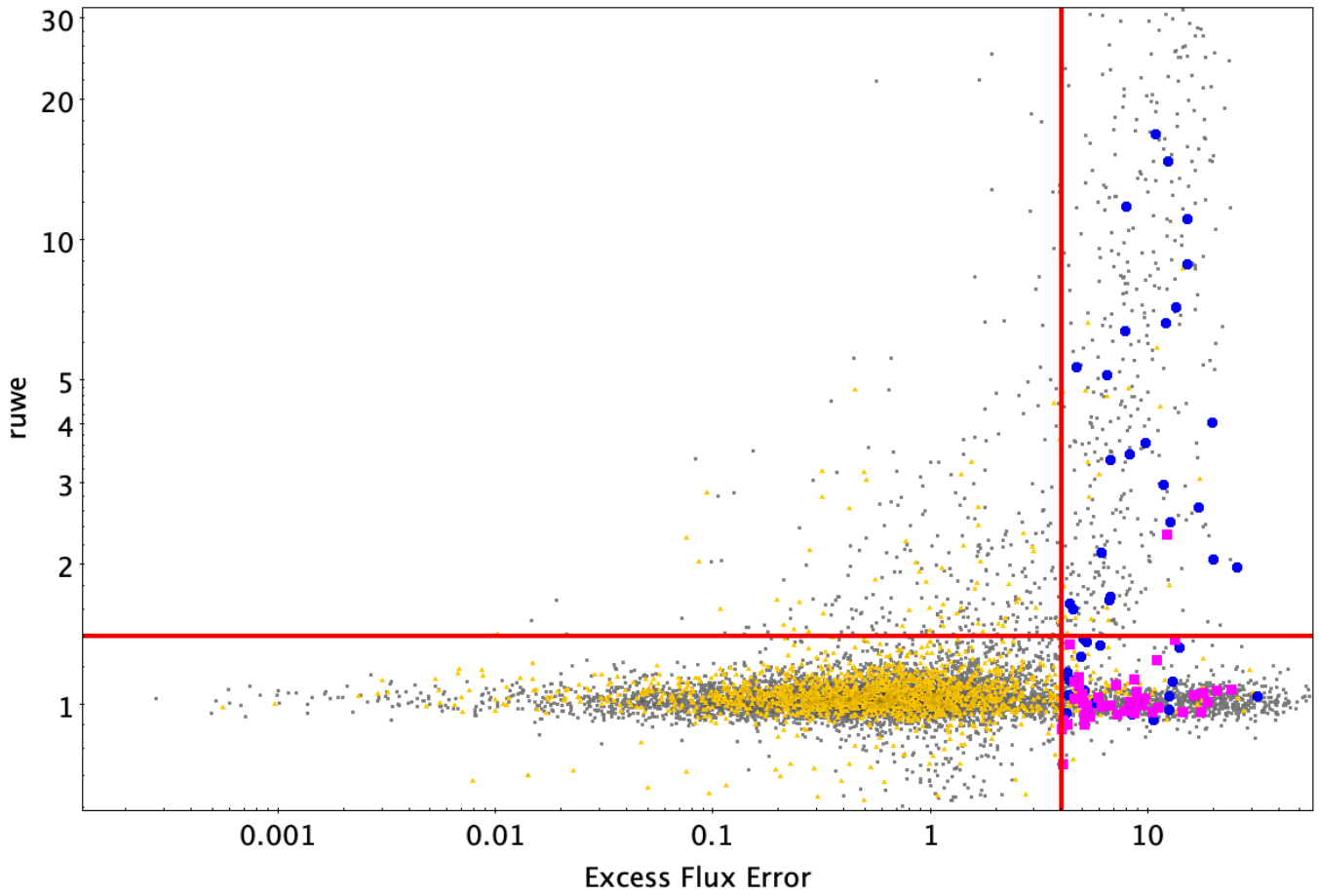

Fig. 11. Excess flux error versus *Gaia* EDR3 (`ruwe`) diagram showing the Final Parallax Selection (grey dots), the known hot subdwarfs in wide binary systems (blue circles), the known hot subdwarfs in close binary systems with WD, dM type, or BD companions (magenta squares), and the known hot subdwarfs where no binarity has been observed (yellow triangles). The red lines shows the variability cutoffs used for (`ruwe`) and flux error excess.

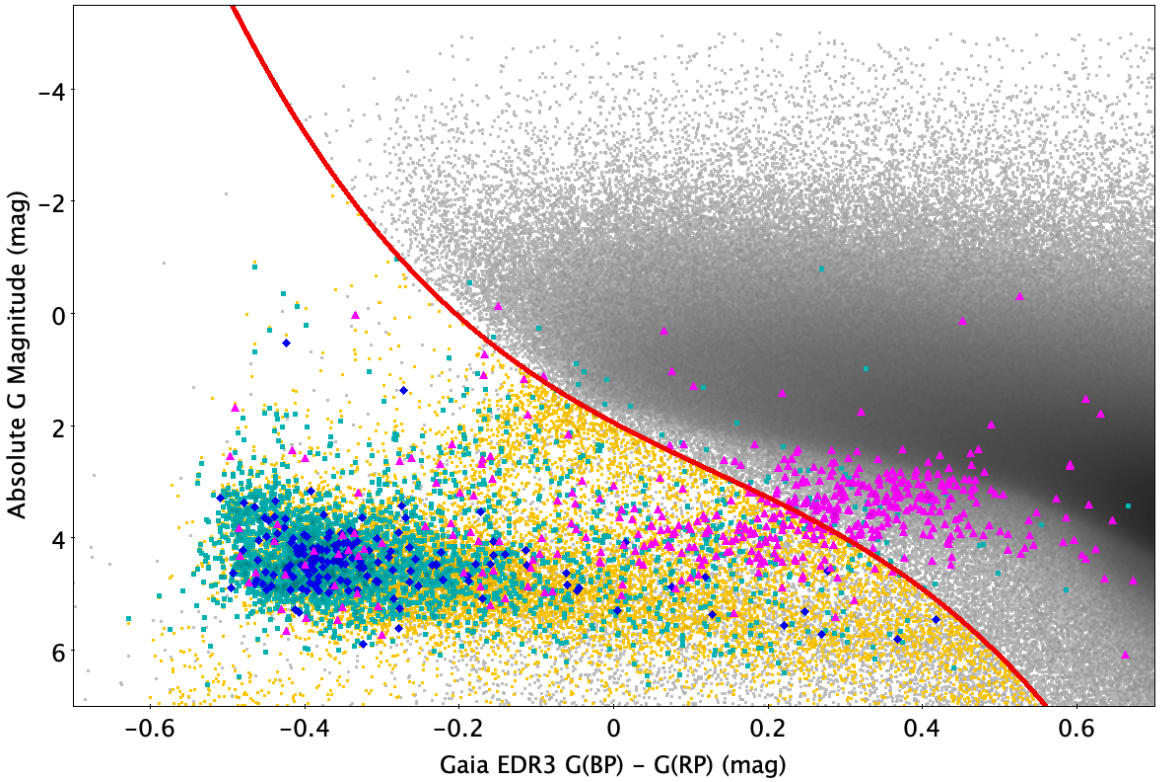

Fig. 12. *Gaia* EDR3 colour–magnitude diagram for the hot subluminous star region showing the initial parallax selection (grey dots), final Parallax Selection (yellow circles), known hot subdwarfs with no binarity observed (cyan squares), known hot subdwarfs in wide binary systems (magenta triangles), and known hot subdwarfs in close binary systems with WD, dwarf-M type or brown dwarf companions (blue diamonds).The red line shows the cutoff used to remove the main sequence region.

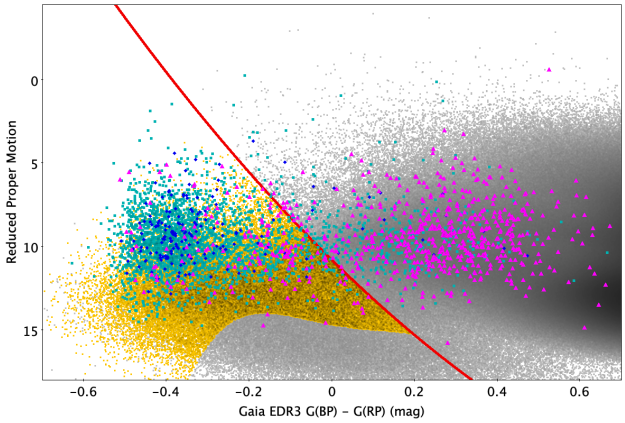

Fig. 13. *Gaia* EDR3 colour reduced proper motion diagram for the hot subluminous star region showing the initial proper motion selection (grey dots), Final Proper Motion Selection (yellow circles), known hot subdwarfs with no binarity observed (cyan squares), known hot subdwarfs in wide binary systems (magenta triangles), and known hot subdwarfs in close binary systems with WD, dwarf-M type or brown dwarf companions (blue diamonds).The red line shows the cutoff used to remove the main sequence region.

In summary, the *Gaia* EDR3 hot subluminous star catalogue parallax selection should be almost complete (80–90%) for single sources and unresolved binaries. However, there is a much lower completeness for hot subdwarfs in wide binary systems as the main sequence companion moves the colour of the binary system away from the EHB cloud in colour–magnitude space. The reduced proper motion selection has a completeness of 50% with a contamination level of 28%.

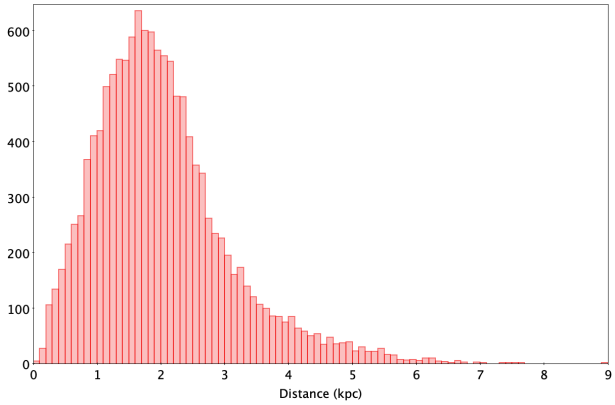

Fig. 14. Distance distribution of the *Gaia* EDR3 Final Parallax Selection objects.

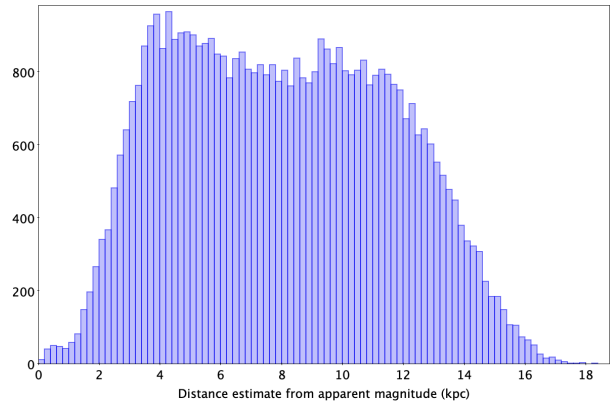

Fig. 15. Approximate distance distribution of the *Gaia* EDR3 Final Proper Motion Selection objects.

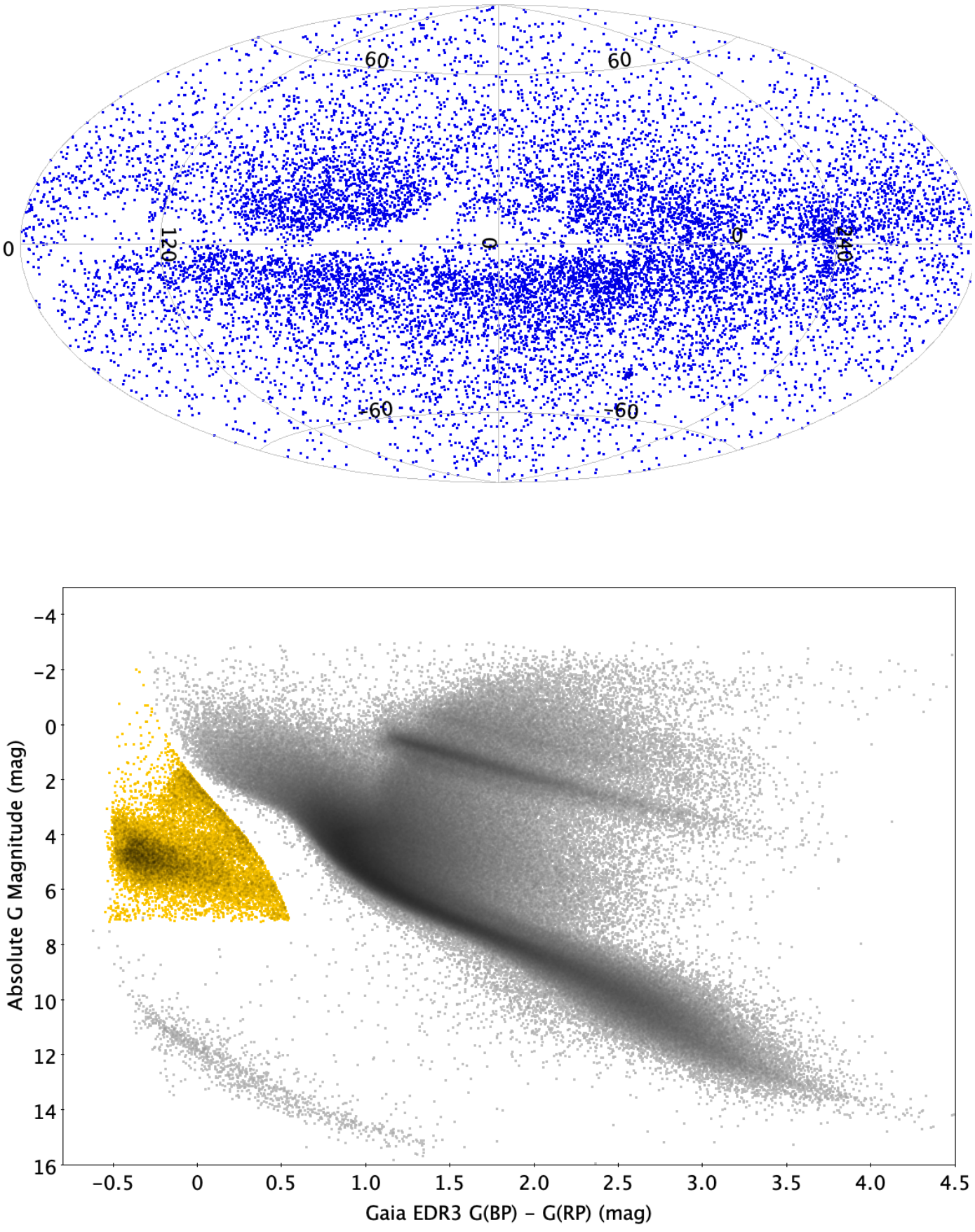

Fig. 16. General properties of the Final Parallax Selection. *Upper panel*: sky distribution of *Gaia* EDR3 Final Parallax Selection objects. *Lower panel*: final Parallax Selection (yellow circles) shown on the full range *Gaia* CMD (grey dots).

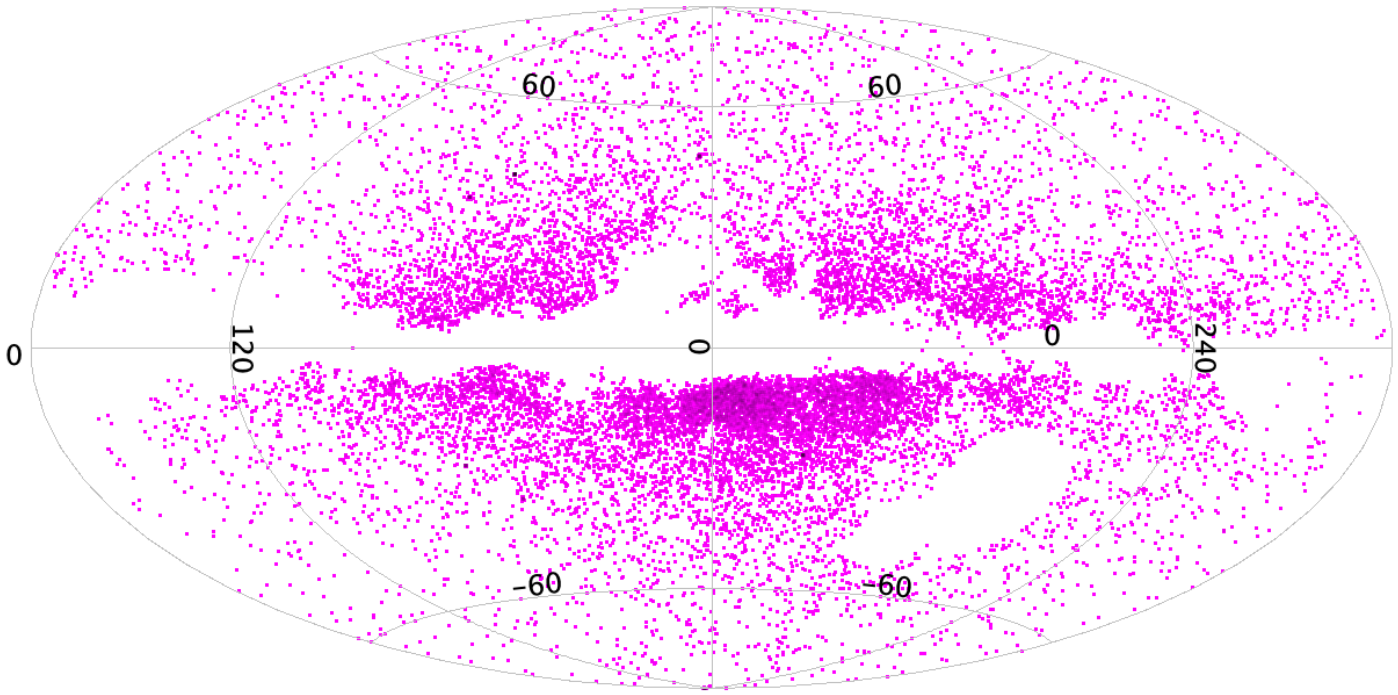

Fig. 17. Sky distribution of *Gaia* EDR3 Final Proper Motion Selection objects.

6. Magnitude, distance, and sky coverage of the catalogues

The *Gaia* EDR3 catalogue of hot subluminous star candidates consists of two parts (for a description of the catalogue columns, see Table B.1). The Final Parallax Selection is a catalogue of 13,123 candidate objects found at distances of up to a few kiloparsecs with an apparent magnitude range from 7.0 up to 18.3 mag with the peak of the distribution at 16.2 mag (see Fig. 18). We consider the Final Parallax Selection to be a full-sky catalogue (see Fig. 16) as there are no filtering or selection criteria based on Galactic latitude or similar. On the other hand, the crowded region filtering does remove some objects in the most crowded regions of the Galactic plane.

The Final Proper Motion Selection catalogue contains 41 822 candidate objects found at approximate distances of up to ~7 kpc with an apparent magnitude range of 8.6 mag up to 19.4 mag with the peak of the distribution at 18 mag (see Fig. 18). The crowded region filtering is stricter than that applied in the Final Parallax Selection and there is also a filter to cut out candidate objects in the direction of the Magellanic Clouds (see Fig. 17).

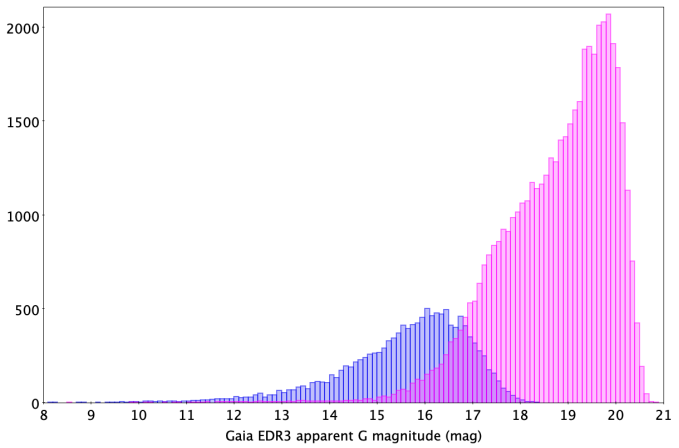

Fig. 18. Distribution of *Gaia* EDR3 apparent *G* magnitude for the Final Parallax Selection (blue) and Final Proper Motion Selection (magenta).

7. Summary and conclusions

In this work, we compiled two catalogues: The Known Hot Subdwarf Catalogue DR3 comprising 6616 known hot subdwarfs with spectroscopic and photometric classifications; and the *Gaia* EDR3 Hot Subluminous Star catalogue comprising 13 123 hot subluminous star candidates with parallax error <20% selected using absolute *G* magnitude and 48 462 hot subluminous star candidates with parallax error ≥20% selected using reduced proper motion.

The known hot subdwarf catalogue DR3 was created using the methods used by Geier (2020) but using the additional, recent discoveries as outlined in Sect. 2.1. The *Gaia* EDR3 Hot Subluminous Star catalogue was generated based on the procedures used in Geier et al. (2019) but modified to take into account the improvements in *Gaia* EDR3 photometry and astrometry compared to *Gaia* DR2. The data quality criteria were also modified to reflect the most recent published methods. The latest colour algorithms were also applied. The improved data quality in *Gaia* EDR3 also meant that we could improve the hot subluminous star candidate detection in the Galactic Plane and, in the Final Parallax Selection, in the direction of the Magellanic Clouds.

For the Final Parallax Selection, we were successful in using astrometric and photometric error excess measurements to discern between main sequence and hot subdwarf binary systems, unresolved hot subdwarf binary systems, and hot subdwarfs not in binary systems.

Our catalogues are the next step in the iterative process of creating a more complete, full-sky catalogue of hot subdwarf

stars. It is known that the colour–magnitude diagram on its own is not sufficient to disentangle the diverse subtypes of hot subluminous stars and to distinguish them without any doubt from main sequence, BHB, and white dwarf stars. Spectroscopic follow-up is needed to learn more about this class of objects.

Our catalogue provides the selection criteria upon which future surveys can be based. In particular, upcoming large spectroscopic surveys (e.g. 4MOST, WEAVE, DESI) can construct their target lists using our catalogue. The target selection for the upcoming 4MOST hot subdwarf (HSD) consortium survey (de Jong et al. 2019) to observe hot subluminous stars in the southern hemisphere will be based on our catalogues.

Acknowledgements. We thank Uli Heber and Harry Dawson for helpful comments and suggestions. IP acknowledges funding by the UK's Science and Technology Facilities Council (STFC), grant ST/T000406/1. This research made use of TOPCAT, an interactive graphical viewer and editor for tabular data Taylor (Taylor 2005). This research made use of the SIMBAD database, operated at CDS, Strasbourg, France; the VizieR catalogue access tool, CDS, Strasbourg, France. Some of the data presented in this paper were obtained from the Mikulski Archive for Space Telescopes (MAST). STScI is operated by the Association of Universities for Research in Astronomy, Inc., under NASA contract NAS5-26555. Support for MAST for non-HST data is provided by the NASA Office of Space Science via grant NNX13AC07G and by other grants and contracts. This research has made use of the services of the ESO Science Archive Facility. This work has made use of data from the European Space Agency (ESA) mission *Gaia* (https://www.cosmos.esa.int/gaia), processed by the *Gaia* Data Processing and Analysis Consortium (DPAC, https://www.cosmos.esa.int/web/gaia/dpac/consortium). Funding for the DPAC has been provided by national institutions, in particular the institutions participating in the *Gaia* Multilateral Agreement. This publication makes use of data products from the Two Micron All Sky Survey, which is a joint project of the University of Massachusetts and the Infrared Processing and Analysis Center/California Institute of Technology, funded by the National Aeronautics and Space Administration and the National Science Foundation. Based on observations made with the NASA Galaxy Evolution Explorer. GALEX is operated for NASA by the California Institute of Technology under NASA contract NAS5-98034. This research has made use of the APASS database, located at the AAVSO web site. Funding for APASS has been provided by the Robert Martin Ayers Sciences Fund. The Guide Star catalogue-II is a joint project of the Space Telescope Science Institute and the Osservatorio Astronomico di Torino. Space Telescope Science Institute is operated by the Association of Universities for Research in Astronomy, for the National Aeronautics and Space Administration under contract NAS5-26555. The participation of the Osservatorio Astronomico di Torino is supported by the Italian Council for Research in Astronomy. Additional support is provided by European Southern Observatory, Space Telescope European Coordinating Facility, the International GEMINI project and the European Space Agency Astrophysics Division. Based on observations obtained as part of the VISTA Hemisphere Survey, ESO Program, 179.A-2010 (PI: McMahon). This publication has made use of data from the VIKING survey from VISTA at the ESO Paranal Observatory, programme ID 179.A-2004. Data processing has been contributed by the VISTA Data Flow System at CASU, Cambridge and WFAU, Edinburgh. Based on data products from observations made with ESO Telescopes at the La Silla Paranal Observatory under program ID 177.A 3011(A,B,C,D,E.F). Based on data products from observations made with ESO Telescopes at the La Silla Paranal Observatory under programme IDs 177.A-3016, 177.A-3017 and 177.A-3018, and on data products produced by Target/OmegaCEN, INAF-OACN, INAF-OAPD and the KiDS production team, on behalf of the KiDS consortium. OmegaCEN and the KiDS production team acknowledge support by NOVA and NWO-M grants. Members of INAF-OAPD and INAF-OACN also acknowledge the support from the Department of Physics & Astronomy of the University of Padova, and of the Department of Physics of Univ. Federico II (Naples). This publication makes use of data products from the Wide-field Infrared Survey Explorer, which is a joint project of the University of California, Los Angeles, and the Jet Propulsion Laboratory/California Institute of Technology, and NEOWISE, which is a project of the Jet Propulsion Laboratory/California Institute of Technology. WISE and NEOWISE are funded by the National Aeronautics and Space Administration. The Pan-STARRS1 Surveys (PS1) and the PS1 public science archive have been made possible through contributions by the Institute for Astronomy, the University of Hawaii, the Pan-STARRS Project Office, the Max-Planck Society and its participating institutes, the Max Planck Institute for Astronomy, Heidelberg and the Max Planck Institute for Extraterrestrial Physics, Garching, The Johns Hopkins University, Durham University, the University of Edinburgh, the Queen's University Belfast, the Harvard-Smithsonian Center for Astrophysics, the Las Cumbres Observatory Global Telescope Network Incorporated, the National Central University of Taiwan, the Space Telescope Science Institute, the National Aeronautics and Space Administration under Grant No. NNX08AR22G issued through the Planetary Science Division of the NASA Science Mission Directorate, the National Science Foundation Grant No. AST-1238877, the University of Maryland, Eotvos Lorand University (ELTE), the Los Alamos National Laboratory, and the Gordon and Betty Moore Foundation. The national facility capability for SkyMapper has been funded through ARC LIEF grant LE130100104 from the Australian Research Council, awarded to the University of Sydney, the Australian National University, Swinburne University of Technology, the University of Queensland, the University of Western Australia, the University of Melbourne, Curtin University of Technology, Monash University and the Australian Astronomical Observatory. SkyMapper is owned and operated by The Australian National University's Research School of Astronomy and Astrophysics. The survey data were processed and provided by the SkyMapper Team at ANU. The SkyMapper node of the All-Sky Virtual Observatory (ASVO) is hosted at the National Computational Infrastructure (NCI). Development and support the SkyMapper node of the ASVO has been funded in part by Astronomy Australia Limited (AAL) and the Australian Government through the Commonwealth's Education Investment Fund (EIF) and National Collaborative Research Infrastructure Strategy (NCRIS), particularly the National eResearch Collaboration Tools and Resources (NeCTAR) and the Australian National Data Service Projects (ANDS). Guoshoujing Telescope (the Large Sky Area Multi-Object Fiber Spectroscopic Telescope LAMOST) is a National Major Scientific Project built by the Chinese Academy of Sciences. Funding for the project has been provided by the National Development and Reform Commission. LAMOST is operated and managed by the National Astronomical Observatories, Chinese Academy of Sciences. Funding for the SDSS and SDSS-II has been provided by the Alfred P. Sloan Foundation, the Participating Institutions, the National Science Foundation, the U.S. Department of Energy, the National Aeronautics and Space Administration, the Japanese Monbukagakusho, the Max Planck Society, and the Higher Education Funding Council for England. The SDSS Web Site is http://www.sdss.org/. The SDSS is managed by the Astrophysical Research Consortium for the Participating Institutions. The Participating Institutions are the American Museum of Natural History, Astrophysical Institute Potsdam, University of Basel, University of Cambridge, Case Western Reserve University, University of Chicago, Drexel University, Fermilab, the Institute for Advanced Study, the Japan Participation Group, Johns Hopkins University, the Joint Institute for Nuclear Astrophysics, the Kavli Institute for Particle Astrophysics and Cosmology, the Korean Scientist Group, the Chinese Academy of Sciences (LAMOST), Los Alamos National Laboratory, the Max-Planck-Institute for Astronomy (MPIA), the Max-Planck-Institute for Astrophysics (MPA), New Mexico State University, Ohio State University, University of Pittsburgh, University of Portsmouth, Princeton University, the United States Naval Observatory, and the University of Washington. Funding for SDSS-III has been provided by the Alfred P. Sloan Foundation, the Participating Institutions, the National Science Foundation, and the U.S. Department of Energy Office of Science. The SDSS-III web site is http://www.sdss3.org/. SDSS-III is managed by the Astrophysical Research Consortium for the Participating Institutions of the SDSS-III Collaboration including the University of Arizona, the Brazilian Participation Group, Brookhaven National Laboratory, University of Cambridge, Carnegie Mellon University, University of Florida, the French Participation Group, the German Participation Group, Harvard University, the Instituto de Astrofisica de Canarias, the Michigan State/Notre Dame/JINA Participation Group, Johns Hopkins University, Lawrence Berkeley National Laboratory, Max Planck Institute for Astrophysics, Max Planck Institute for Extraterrestrial Physics, New Mexico State University, New York University, Ohio State University, Pennsylvania State University, University of Portsmouth, Princeton University, the Spanish Participation Group, University of Tokyo, University of Utah, Vanderbilt University, University of Virginia, University of Washington, and Yale University. Funding for the Sloan Digital Sky Survey IV has been provided by the Alfred P. Sloan Foundation, the U.S. Department of Energy Office of Science, and the Participating Institutions. SDSS-IV acknowledges support and resources from the Center for High Performance Computing at the University of Utah. The SDSS website is www.sdss.org. SDSS-IV is managed by the Astrophysical Research Consortium for the Participating Institutions of the SDSS Collaboration including the Brazilian Participation Group, the Carnegie Institution for Science, Carnegie Mellon University, Center for Astrophysics | Harvard & Smithsonian, the Chilean Participation Group, the French Participation Group, Instituto de Astrofísica de Canarias, The Johns Hopkins University, Kavli Institute for the Physics and Mathematics of the Universe (IPMU) / University of Tokyo, the Korean Participation Group, Lawrence Berkeley National Laboratory, Leibniz Institut für Astrophysik Potsdam (AIP), Max-Planck-Institut für Astronomie (MPIA Heidelberg), Max-Planck-Institut für Astrophysik (MPA Garching), Max-Planck-Institut für Extraterrestrische Physik (MPE), National Astronomical Observatories of China, New Mexico State University, New York University, University of Notre Dame, Observatário Nacional / MCTI, The Ohio

State University, Pennsylvania State University, Shanghai Astronomical Observatory, United Kingdom Participation Group, Universidad Nacional Autónoma de México, University of Arizona, University of Colorado Boulder, University of Oxford, University of Portsmouth, University of Utah, University of Virginia, University of Washington, University of Wisconsin, Vanderbilt University, and Yale University.

References

Adams, W. S., Joy, A. H., Humason, M. L., & Ada, M. 1935, ApJ, 81, 191
Ahmad, A., & Jeffery, C. S. 2003, A&A, 402, 335
Alam, S., Albareti, F. D., Allende Prieto, C., et al. 2015, ApJS, 219, 12
Aller, A., Montesinos, B., Miranda, L. F., Solano, F., & Ulla, A. 2015, MNRAS, 448, 2822
Almeida, L. A., Jablonski, F., Tello, J., & Rodrigues, C. V. 2012, MNRAS, 423, 478
Bachulski, S., Baran, A. S., Jeffery, C. S., et al. 2016, AcA, 66, 455
Baran, A. S., Reed, M. D., Stello, D., et al. 2012, MNRAS, 424, 2686
Baran, A. S., Telting, J. H., Nemeth, P., et al. 2016, A&A, 585, A66
Baran, A. S., Telting, J. H., Jeffery, C. S., et al. 2019, MNRAS, 489, 1556
Barlow, B. N., Dunlap, B. H., Clemens, J. C., et al. 2010, MNRAS, 403, 324
Barlow, B. N., Kilkenny, D., Drechsel, H., et al. 2013, MNRAS, 430, 22
Bauer, F., & Husfeld, D. 1995, A&A, 300, 481
Bell, K. J., Kosakowski, A., Kilic, M., et al. 2019, Res. Notes Am. Astron. Soc., 3, 81
Belokurov, V., Penoyre, Z., Semyeong, O., et al. 2020, MNRAS, 496, 1922
Berger, J., & Fringant, A. M. 1984, A&AS, 58, 565
Bixler, J. V., Bowyer, S., & Laget, M. 1991, A&A, 250, 370
Bloemen, S., Marsh, T. R., Østensen, R. H., et al. 2011, MNRAS, 410, 1787
Brown, W. R., Geller, M. J., & Kenyon, S. J. 2014, ApJ, 787, 89
Burleigh, M. R., Heber, U., O'Donoghue, D., & Barstow, M. A. 2000, A&A, 356, 585
Charpinet, S., van Grootel, V., Reese, D., et al. 2008, A&A, 489, 377
Charpinet, S., Green, E. M., Baglin, A., et al. 2010, A&A, 516, L6
Chavira, E. 1958, Bol. Obs. Tonantz. Tacub., 2, 15
Chavira, E. 1959, Bol. Obs. Tonantz. Tacub., 2, 3
Chayer, P., Dixon, W. V., Fullerton, A. W., Ooghe-Tabanou, B., & Reid, I. N. 2015, MNRAS, 452, 2292
Chornay, N., Walton, N. A., Jones, D., et al. 2015, A&A, 468, A95
Copperwheat, C. M., Morales-Rueda, L., Marsh, T. R., Maxted, P. F. L., & Heber, U. 2011, MNRAS, 415, 1318
Culpan, R., Geier, S., & Pelisoli, I.. 2020, A&A, 654, A107
de Marco, O., Long, J., Jacoby, G. H., et al. 2015, MNRAS, 448, 3587
de Jong, R. S., Agertz, O., Agudo Berbel, A., et al. 2019, The Messenger, 175, 3
Demers, S., Beland, S., Kibblewhite, E. J., Irwin, M. J., & Nithakorn, D. S. 1986, AJ, 92, 878
Derekas, A., Nemeth, P., Southworth, J., et al. 2015, ApJ, 808, 179
Dorsch, M., Reindl, N., Pelisoli, I., et al. 2022, A&A, 658, L9
Downes, R. A. 1986, ApJS, 61, 569
Dreizler, S. 1998, Balt. Astron., 7, 71
Dreizler, S., Heber, U., Werner, K., Moehler, S., & de Boer, K. S. 1990, A&A, 235, 234
Edelmann, H., Heber, U., Napiwotzki, R., Reid, I. N., & Saffer, R. A. 1999, ASP Conf. Ser. 169, 546
Edelmann, H., Heber, U., Hagen, H.-J., et al. 2003, A&A, 400, 939
Fabricius, C., Luri, X., Arenou, F., Babusiaux, C., Helmi, A., et al. 2020, A&A, 649, A5
Feige, J. 1958, ApJ, 128, 267
Fontaine, M., Chayer, P., Oliveira, C. M., Wesemael, F., & Fontaine, G. 2008, ApJ, 678, 394
For, B.-Q., Green, E. M., Fontaine, G., et al. 2010, ApJ, 708, 253
Frew, D. J., Bojicic, I. S., Parker, Q. A., et al. 2014, MNRAS, 440, 1345
Gaia Collaboration (Brown, A.G.A., et al.) 2018, A&A, 616, A1
Gaia Collaboration (Brown, A.G.A., et al.) 2021a, A&A, 649, A1
Gaia Collaboration (Brown, A.G.A., et al.) 2021b, A&A, 650, C3
Geier, S. 2015, Astron. Nachr., 336, 437
Geier, S. 2020, A&A, 635, A193
Geier, S., Nesslinger, S., Heber, U., et al. 2008, A&A, 477, L13
Geier, S., Heber, U., Podsiadlowki, Ph., et al. 2010, A&A, 519, A25
Geier, S., Hirsch, H., Tillich, A., et al. 2011, A&A, 530, A28
Geier, S., Heber, U., Edelmann, H., et al. 2013a, A&A, 557, A122
Geier, S., Marsh, T. R., Wang, B., et al. 2013b, A&A, 554, A54
Geier, S., Østensen, R. H., Heber, U., et al. 2014, A&A, 562, A95
Geier, S., Fürst, F., Ziegerer, E., et al. 2015a, Science, 347, 1126
Geier, S., Kupfer, T., Heber, U., et al. 2015b, A&A, 577, A26
Geier, S., Østensen, R. H., Nemeth, P., et al. 2017a, A&A, 600, A50
Geier, S., Østensen, R. H., Nemeth, P., et al. 2017b, Open Astron., 26, 164
Geier, S., Raddi, R., Gentile Fusillo, N. P., & Marsh, T. R. 2019, A&A, 621, A38
Geier, S., Dorsch, M., Pelisoli, I., et al. 2022, A&A, 661, A113
Gentile Fusillo, N. P., Tremblay, P.-E., Gänsicke, B. T., et al. 2019, MNRAS, 482, 4570
Gentile Fusillo, N. P., Tremblay, P.-E., Cukanovaite, E., et al. 2021, MNRAS, 508, 3877
Giddings, J. R. 1981, PhD thesis, University of London, UK
Green, R. F., Schmidt, M., & Liebert, J. 1986, ApJS, 61, 305
Greenstein, J. L. 1973, A&A, 23, 1
Guidry, J. A., Vanderbosch, Z. P., Hermes, J. J., et al. 2021, ApJ, 912, 125
Gvaramadze, V. V., Gräfener, G., Langer, N., et al. 2019, Nature, 569, 684
Hagen, H.-J., Groote, D., Engels, D., & Reimers, D. 1995, A&AS, 111, 195
Han, Z., Podsiadlowski, P., Maxted, P. F. L., Marsh, T. R., & Ivanova, N. 2002, MNRAS, 336, 449
Han, Z., Podsiadlowski, P., Maxted, P. F. L., & Marsh, T. R. 2003, MNRAS, 341, 669
Haro, G., & Luyten, W. J. 1962, Bol. Obs. Tonantz. Tacub., 3, 37
Heber, U. 1986, A&A, 155, 33
Heber, U. 2016, PASP, 128, 082001
Heber, U., & Hunger, K. 1987, The Messenger, 47, 36
Heber, U., & Kudritzki, R. P. 1986, A&A, 169, 244
Heber, U., & Langhans, G. 1986, ESA SP, 263, 279
Heber, U., Hunger, K., Jonas, G., & Kudritzki, R. P. 1984, A&A, 130, 119
Heber, U., Kudritzki, R. P., Caloi, V., et al. 1986, A&A, 162, 171
Heber, U., Moehler, S., Napiwotzki, R., Thejll, P., & Green, E. M. 2002, A&A, 383, 938
Heber, U., Edelmann, H., Lisker, T., & Napiwotzki, R. 2003, A&A, 411, L477
Herald, J. E., & Bianchi, L. 2011, MNRAS, 417, 2440
Hillwig, T. C., Frew, D. J., Reindl, R., et al. 2017, AJ, 153, 24
Hirsch, H. 2009, PhD thesis, Friedrich-Alexander University Erlangen-Nürnberg, Germany
Hogg, M. A., Casewell, S. L., Wynn, G. A., et al. 2020, MNRAS, 498, 12
Holdsworth, D. L., Østensen, R. H., Smalley, B., & Telting, J. H. 2017, MNRAS, 466, 502
Hügelmeyer, S., Dreizler, S., Homeier, D., et al. 2006, A&A, 454, 617
Humason, M. L., & Zwicky, F. 1947, ApJ, 105, 85
Hunger, K., Gruschinske, J., Kudritzki, R. P., & Simon, K. P. 1981, A&A, 95, 244
Husfeld, D., Butler, K., Heber, U., & Drilling, J. S. 1989, A&A, 222, 150
Iriarte, B., & Chavira, E. 1957, Bol. Obs. Tonantz. Tacub., 2, 3
Jeffery, C. S., & Hamann, W.-R. 2010, MNRAS, 404, 1698
Jeffery, C. S., Simon, T., & Lloyd Evans, T. 1992, MNRAS, 258, 64
Jeffery, C. S., Ramsay, G., Naslim, N., et al. 2013, MNRAS, 429, 3207
Jeffery, C. S., Miszalski, B., & Snowdon, E. 2021, MNRAS, 501, 623
Kepler, S. O., Pelisoli, I., Koester, D., et al. 2015, MNRAS, 446, 4078
Kepler, S. O., Pelisoli, I., Koester, D., et al. 2016, MNRAS, 455, 3413
Kepler, S. O., Pelisoli, I., Koester, D., et al. 2019, MNRAS, 486, 2169
Kilkenny, D., Heber, U., & Drilling, J. S. 1988, SAAOC, 12, 1
Kilkenny, D., Worters, H. L., & Lynas-Gray, A. E. 2019, MNRAS, 485, 4330
Klepp, S., & Rauch, T. 2011, A&A, 531, L7
Koen, C. 2011, MNRAS, 415, 3042
Koen, C., Orosz, J. A., & Wade, R. A. 1998, MNRAS, 300, 695
Kreuzer, S. 2021, PhD thesis, University of Erlangen-Nürnberg, Germany
Kuiper, G. P. 1939, ApJ, 89, 548
Kupfer, T., Geier, S., Schaffenroth, V., et al. 2015, A&A, 576, A44
Kupfer, T., Ramsay, G., van Roestel, J., et al. 2017a, ApJ, 851, 28
Kupfer, T., van Roestel, J., Brooks, J., et al. 2017b, ApJ, 835, 131
Kupfer, T., Bauer, E. B., Marsh, T. R., et al. 2020, ApJ, 891, 45
Kupfer, T., Bauer, E. B., van Roestel, J., et al. 2022, ApJ, 925, L12
Lanz, T., Hubeny, I., & Heap, S. R. 1997, ApJ, 485, 843
Latour, M., Fontaine, G., Brassard, P., et al 2011, ApJ, 733, 100
Latour, M., Fontaine, G., Green, E. M., & Brassard, P. 2015, A&A, 579, A39
Latour, M., Chayer, P., Green, E. M., Irrgang, A., & Fontaine, G. 2018a, A&A, 609, A89
Latour, M., Randall, S. K., Calamida, A., Geier, S., & Moehler, S. 2018b, A&A, 618, A15
Lei, Z., Zhao, J., Nemeth, P., & Zhao, G. 2018, ApJ, 868, 70
Lei, Z., Zhao, J., Nemeth, P., & Zhao, G. 2019, ApJ, 881, 135
Lei, Z., Zhao, J., Nemeth, P., & Zhao, G. 2020, ApJ, 889, 117
Lemke, M., Heber, U., Napiwotzki, R., Dreizler, S., & Engels, D. 1997, The Third Conference on Faint Blue Stars, eds. A. G. D. Philip, J. Liebert, R. Saffer & D. S. Hayes (L. Davis Press), 375

Lindegren, L., Hernandez, J., Bombrun, A., et al. 2018, A&A, 616, A2
Lindegren, L., Klioner, S. A., Hernandez, J., et al. 2021a, A&A, 649, A2
Lindegren, L., Bastian, U., Biermann, M., et al. 2021b, A&A, 649, A4
Lisker, T., Heber, U., Napiwotzki, R., Christlieb, N., Han, Z., et al. 2005, A&A, 430, 223
Löbling, L. 2020, MNRAS, 497, 67
Löbling, L., Rauch, T., Miller Bertolami, M. M., et al. 2019, MNRAS, 489, 1054
Luo, Y.-P., Nemeth, P., Liu, C., Deng, L.-C., & Han, Z. 2016, ApJ, 818, 202
Luo, Y.-P., Nemeth, P., Deng, L.-C., & Han, Z. 2019, ApJ, 881, 7
Luo, Y.-P., Nemeth, P., Wan, K., Wang, X., & Han, Z. 2021, ApJS, 256, 28
Luyten, W. J. 1953, AJ, 58, 75
Luyten, W. J., & Miller, W. C. 1951, ApJ, 114, 488
Lynas-Gray, A. E. 2004, Ap&SS, 291, 197
Maxted, P. F. L., Heber, U., Marsh, T. R., & North, R. C. 2001, MNRAS, 326, 139
Maxted, P. F. L., Marsh, T. R., Heber, U., et al. 2002, MNRAS, 333, 231
McMahon, R. G., Banerji, M., Gonzalez, E., et al. 2013, The Messenger, 154, 35
Mickaelian, A. M. 2008, AJ, 136, 946
Mickaelian, A. M., Nesci, R., Rossi, C., et al. 2007, A&A, 464, 1177
Miszalski, B., Crowther, P. A., de Marco, O., et al. 2012, MNRAS, 423, 934
Moehler, S., Heber, U., & de Boer, K. 1990, A&A, 239, 265
Moni Bidin, C., Moehler, S., Piotto, G., Momany, Y., & Recio-Blanco, A. 2007, A&A, 474, 505
Moni Bidin, C., Moehler, S., Piotto, G., Momany, Y., & Recio-Blanco, A. 2009, A&A, 498, 737
Moni Bidin, C., Villanova, S., Piotto, G., et al. 2012, A&A, 547, A109
Morales-Rueda, L., Maxted, P. F. L., Marsh, T. R., North, R. C., & Heber, U. 2003, MNRAS, 338, 752
Mowlavi, N., Rimoldini, L., Evans, D. W., et al. 2021, A&A, 648, A44
Napiwotzki, R. 1999, A&A, 350, 101
Naslim, N., Jeffery, C. S., Ahmad, A., Behara, N. T., & Sahin, T. 2010, MNRAS, 409, 582
Nemeth, P., Kawka, A., & Vennes, S. 2012, MNRAS, 427, 2180
Nemeth, P., Ziegerer, E., Irrgang, A., et al. 2016, ApJ, 821, L13
Østensen, R. H., 2006, Balt. Astron., 15, 85
Østensen, R. H., Green, E. M., Bloemen, S., et al. 2010a, MNRAS, 408, 51
Østensen, R. H., Oreiro, R., Solheim, J.-E., et al. 2010b, A&A, 513, A6
Østensen, R. H., Silvotti, R., Charpinet, S., et al. 2010c, MNRAS, 409, 1470
Østensen, R. H., Reed, M. D., Baran, A. S., & Telting, J. H. 2014, A&A, 564, L14
O'Toole, S. J., & Heber, U. 2006, A&A, 452, 579
Pelisoli, I., & Vos, J. 2019, MNRAS, 488, 2892
Pelisoli, I., Vos, J., Geier, s., Schaffenroth, V., & Baran, A. S., 2020, A&A 642, A180
Pelisoli, I., Neunteufel, P., Geier, S., et al. 2021, Nat. Astron. 5, 1052
Penoyre, Z., Belokurov, V., Wyn Evans, N. 2021, MNRAS, 513, 2437
Przybilla, N., Nieva, M. F., & Edelmann, H. 2006, Balt. Astron., 15, 107
Ramspeck, M., Heber, U., & Edelmann, H. 2001, A&A, 379, 235
Ratzloff, J. K., Barlow, B. N., Kupfer, T., et al. 2019, ApJ, 883, 51
Ratzloff, J. K., Kupfer, T., Barlow, B. N., et al. 2020, ApJ, 902, 92
Rauch, T. 1993, A&A, 276, 171
Rauch, T., & Werner, K. 1995, Lect. Notes Phys., 443, 186
Rauch, T., Heber, U., Hunger, K., Werner, K., & Neckel, T. 1991, A&A, 241, 457
Rauch, T., Rudkowski, A., Kampka, D., et al. 2014, A&A, 566, A3
Reindl, N., Rauch, T., Werner, K., Kruk, J. W., & Todt, H. 2014, A&A, 566, A116
Reindl, N., Geier, S., Kupfer, T., et al. 2016, A&A, 587, A101
Reindl, R., Rauch, T., Miller Bertolami, M. M., Todt, H., & Werner, K. 2017, MNRAS, 464, 51
Reindl, N., Schaffenroth, V., Miller Bertolami, M. M., et al. 2020, A&A, 638, A93
Riello, M., De Angeli, F., Evans, D. W., et al. 2021, A&A, 649, A3
Saffer, R. A., Bergeron, P., Koester, D., & Liebert, J. 1994, ApJ, 432, 351
Saffer, R. A., Keenan, F. P., Hambly, N. C., Dufton, P. L., & Liebert, J. 1997, ApJ, 491, 172
Schaffenroth, V., Geier, S., Drechsel, H., et al. 2013, A&A, 553, A18
Schaffenroth, V., Barlow, B. N., Geier S., et al. 2019, A&A, 630, A80
Schaffenroth, V., Casewell, S. L., Schneider, D., et al. 2021, MNRAS, 501, 3874
Silvotti, R., Schaffenroth, V., Heber, U., et al. 2021, MNRAS, 500, 2461
Silvotti, R., Nemeth, P., Telting, J. H., et al. 2022, MNRAS, 511, 2, 2201
Slettebak, A., & Brundage R. K. 1971, AJ, 76, 338
Stobie, R. S., Kilkenny, D., O'Donoghue, D., et al. 1997, MNRAS, 287, 848
Ströer, A., Heber, U., Lisker, T., et al. 2007, A&A, 462, 269
Taylor, M. B. 2005, ASP Conf. Ser., 347, 29
Theissen, A., Moehler, S., Heber, U., & de Boer, K. S. 1993, A&A, 273, 524
Thejll, P., Bauer, F., Saffer, R., et al. 1994, ApJ, 433, 819
Tillich, A., Heber, U., Geier, S., et al. 2011, A&A, 527, A137
Todt, H. 2009, PhD thesis, University of Potsdam, Germany
Tomley, L. 1970, ApJ, 162, 239
van Grootel, V., Charpinet, S., Fontaine, G., et al. 2010, ApJ, 718, 97
Vennes, S., Kawka, A., & Németh, P. 2011, MNRAS, 410, 2095
Verbeek, K., Groot, P. J., Scaringi, S., et al. 2012, MNRAS, 426, 1235
Viton, M., Deleuil, M., Tobin, W., Prevot, L., & Bouchet, P. 1991, A&A, 242, 175
Vos, J., Østensen, R. H., Degroote, P., et al. 2012, A&A, 548, A6
Vos, J., Østensen, R. H., Nemeth, P., et al. 2013, A&A, 559, A54
Vos, J., Nemeth, P., Vuckovic, M., Østensen, R. H., & Parsons, S. 2018, MNRAS, 473, 693
Vos, J., Pelisoli, I., Budaj, J., et al. 2021, A&A, 655, A43
Weidmann, W. A., Mari, M. B., Schmidt, E. O., et al. 2020, A&A, 640, A10
Werner, K., & Rauch, T. 2015, A&A, 583, A131
Werner, K., Rauch, T., Napiwotzki, R., et al. 2004a, A&A, 2004, 424, 657
Werner, K., Rauch, T., Reiff, E., Kruk, J. W., & Napiwotzki, R. 2004b, A&A, 427, 685
Werner, K., Rauch, T., & Kruk, J. W. 2005, A&A, 433, 641
Werner, K., Rauch, T., & Kepler, S. O. 2014, A&A, 564, A53
Werner, K., Reindl, N., Dorsch, M., et al. 2022a, A&A, 658, A66
Werner, K., Reindl, N., Geier, S., et al. 2022b, MNRAS, in press
Wisotzki, L., Koehler, T., Groote, D., & Reimers, D. 1996, A&AS, 115, 227
Wood, J. H., & Saffer, R. A. 1999, MNRAS, 305, 820
Ziegerer, E., Heber, U., Geier, S., et al. 2017, A&A, 601, A58
Ziegler, M. 2012, PhD thesis, University of Tübingen, Germany

Appendix A: Catalogue of known hot subdwarfs DR3

Table A.1. Catalogue columns

Column	Format	Description	Unit
NAME	A30	Target name	
GAIA_DESIG	A30	Gaia designation	
RA	F10.6	Right ascension (J2000)	deg
DEC	F10.6	Declination (J2000)	deg
GLON	F10.6	Galactic longitude	deg
GLAT	F10.6	Galactic latitude	deg
SPEC_CLASS	A15	Spectroscopic classification	
SPEC_SIMBAD	A15	Spectroscopic classification from SIMBAD	
COLOUR_SDSS	A10	Colour classification SDSS	
COLOUR_APASS	A10	Colour classification GALEX/APASS	
COLOUR_PS1	A10	Colour classification GALEX/PS1	
COLOUR_SKYM	A10	Colour classification SkyMapper	
PLX	F8.4	Gaia parallax	mas
PLX_ZP	F8.4	Zero-point-corrected Gaia parallax	mas
e_PLX	F8.4	Error on PLX	mas
M_G	F8.4	Absolute magnitude in G-band	mag
G_GAIA	F6.3	Gaia G-band magnitude	mag
e_G_GAIA	F6.3	Error on G_GAIA	mag
BP_GAIA	F6.3	Gaia BP-band magnitude	mag
e_BP_GAIA	F6.3	Error on BP_GAIA	mag
RP_GAIA	F6.3	Gaia RP-band magnitude	mag
e_RP_GAIA	F6.3	Error on RP_GAIA	mag
PMRA_GAIA	F7.3	Gaia proper motion $\mu_\alpha \cos\delta$	mas yr^{-1}
e_PMRA_GAIA	F7.3	Error on PMRA_GAIA	mas yr^{-1}
PMDEC_GAIA	F7.3	Gaia proper motion μ_δ	mas yr^{-1}
e_PMDEC_GAIA	F7.3	Error on PMDEC_GAIA	mas yr^{-1}
RV_SDSS	F5.1	Radial velocity SDSS	km s^{-1}
e_RV_SDSS	F5.1	Error on RV_SDSS	km s^{-1}
RV_LAMOST	F5.1	Radial velocity LAMOST	km s^{-1}
e_RV_LAMOST	F5.1	Error on RV_LAMOST	km s^{-1}
TEFF	F8.1	Effective temperature	K
e_TEFF	F8.1	Error on T_EFF	K
LOG_G	F4.2	Log surface gravity (gravity in cm s^{-2})	dex
e_LOG_G	F.4.2	Error on LOG_G	dex
LOG_Y	F5.2	Log helium abundance n(He)/n(H)	dex
e_LOG_Y	F5.2	Error on LOG_Y	dex
PARAMS_REF	A20	Reference for atmospheric parameters (Bibcode)[1]	
EB-V	F6.4	Interstellar reddening E(B-V)	mag
e_EB-V	F6.4	Error on EB-V	mag
AV	F6.4	Interstellar extinction A_V	mag
FUV_GALEX	F6.3	GALEX FUV-band magnitude	mag

[1] References from the literature: Tomley (1970); Greenstein (1973); Giddings (1981); Hunger et al. (1981); Heber et al. (1984); Heber & Kudritzki (1986); Heber et al. (1986); Heber & Langhans (1986); Heber (1986); Heber et al. (1987, 2002, 2003); Husfeld et al. (1989); Dreizler et al. (1990); Moehler et al. (1990); Bixler et al. (1991); Rauch et al. (1991, 2014); Viton et al. (1991); Jeffery et al. (1992, 2013, 2021); Rauch (1993); Theissen et al. (1993); Saffer et al. (1994, 1997); Thejll et al. (1994); Bauer et al. (1995); Rauch & Werner (1995); Lanz et al. (1997); Lemke et al. (1997); Dreizler (1998); Koen et al. (1998); Napiwotzki (1999); Edelmann et al. (1999); Wood & Saffer (1999); Burleigh et al. (2000); Maxted et al. (2001); Ramspeck et al. (2001); Maxted et al. (2002); Ahmad & Jeffery (2003); Edelmann et al. (2003); Morales-Rueda et al. (2003); Werner et al. (2004a,b, 2005, 2014); Werner & Rauch (2015); Werner et al. (2022a,b); Lisker et al. (2005); O'Toole & Heber (2006); Hügelmeyer et al. (2006); Przybilla et al. (2006); Moni Bidin et al. (2007, 2009, 2012); Ströer et al. (2007); Charpinet et al. (2008, 2010); Geier et al. (2008, 2010, 2011); Geier et al. (2013a,b, 2014, 2015b, 2017b); Geier et al. (in prep.); Geier et al. (2022); Fontaine et al. (2008); Hirsch (2009); Todt (2009); For et al. (2010); van Grootel et al. (2010); Barlow et al. (2010, 2013); Jeffery et al. (2010); Naslim et al. (2010); Østensen et al. (2010a,b,c, 2014); Klepp & Rauch (2011); Latour et al. (2011, 2015, 2018a); Tillich et al. (2011); Bloemen et al. (2011); Copperwheat et al. (2011); Koen (2011); Herald & Bianchi (2011); Miszalski et al. (2008); Nemeth et al. (2012, 2016); Vos et al. (2012); Vos et al (2013); Almeida et al. (2012); Baran et al. (2012, 2016, 2019); Verbeek et al. (2012); Ziegler (2012); Schaffenroth et al. (2013, 2019, 2021); Frew et al. (2014); Reindl et al. (2014); Kupfer et al. (2015, 2017a,b, 2020, 2022); Kepler et al. (2016, 2019); Reindl et al. (2016, 2017, 2020); Derekas et al. (2015); Chayer et al. (2015); de Marco et al. (2015); Aller et al. (2015); Bachulski et al. (2016); Luo et al. (2016, 2019, 2021); Ziegerer et al. (2017); Hillwig et al. (2017); Holdsworth et al. (2017); Lei et al. (2018, 2019, 2020); Gvaramadze et al. (2019); Ratzloff et al. (2019, 2020); Kilkenny et al. (2019); Löbling et al. (2019); Bell et al. (2019); Löbling (2020); Hogg et al. (2020); Silvotti et al. (2021, 2022); Pelisoli et al. (2021); Dorsch et al. (2022)

e_FUV_GALEX	F6.3	Error on FUV_GALEX	mag
NUV_GALEX	F6.3	GALEX NUV-band magnitude	mag
e_NUV_GALEX	F6.3	Error on NUV_GALEX	mag
V_APASS	F6.3	APASS V-band magnitude	mag
e_V_APASS	F6.3	Error on V_APASS	mag
B_APASS	F6.3	APASS B-band magnitude	mag
e_B_APASS	F6.3	Error on V_APASS	mag
g_APASS	F6.3	APASS g-band magnitude	mag
e_g_APASS	F6.3	Error on g_APASS	mag
r_APASS	F6.3	APASS r-band magnitude	mag
e_r_APASS	F6.3	Error on r_APASS	mag
i_APASS	F6.3	APASS i-band magnitude	mag
e_i_APASS	F6.3	Error on i_APASS	mag
u_SDSS	F6.3	SDSS u-band magnitude	mag
e_u_SDSS	F6.3	Error on u_SDSS	mag
g_SDSS	F6.3	SDSS g-band magnitude	mag
e_g_SDSS	F6.3	Error on g_SDSS	mag
r_SDSS	F6.3	SDSS r-band magnitude	mag
e_r_SDSS	F6.3	Error on r_SDSS	mag
i_SDSS	F6.3	SDSS i-band magnitude	mag
e_i_SDSS	F6.3	Error on i_SDSS	mag
z_SDSS	F6.3	SDSS z-band magnitude	mag
e_z_SDSS	F6.3	Error on z_SDSS	mag
u_VST	F6.3	VST surveys (ATLAS, KiDS) u-band magnitude	mag
e_u_VST	F6.3	Error on u_VST	mag
g_VST	F6.3	VST surveys (ATLAS, KiDS) g-band magnitude	mag
e_g_VST	F6.3	Error on g_VST	mag
r_VST	F6.3	VST surveys (ATLAS, KiDS) r-band magnitude	mag
e_r_VST	F6.3	Error on r_VST	mag
i_VST	F6.3	VST surveys (ATLAS, KiDS) i-band magnitude	mag
e_i_VST	F6.3	Error on i_VST	mag
z_VST	F6.3	VST surveys (ATLAS, KiDS) z-band magnitude	mag
e_z_VST	F6.3	Error on z_VST	mag
u_SKYM	F6.3	SkyMapper u-band magnitude	mag
e_u_SKYM	F6.3	Error on u_SKYM	mag
v_SKYM	F6.3	SkyMapper v-band magnitude	mag
e_v_SKYM	F6.3	Error on v_SKYM	mag
g_SKYM	F6.3	SkyMapper g-band magnitude	mag
e_g_SKYM	F6.3	Error on g_SKYM	mag
r_SKYM	F6.3	SkyMapper r-band magnitude	mag
e_r_SKYM	F6.3	Error on r_SKYM	mag
i_SKYM	F6.3	SkyMapper i-band magnitude	mag
e_i_SKYM	F6.3	Error on i_SKYM	mag
z_SKYM	F6.3	SkyMapper z-band magnitude	mag
e_z_SKYM	F6.3	Error on z_SKYM	mag
g_PS1	F7.4	PS1 g-band magnitude	mag
e_g_PS1	F7.4	Error on g_PS1	mag
r_PS1	F7.4	PS1 r-band magnitude	mag
e_r_PS1	F7.4	Error on r_PS1	mag
i_PS1	F7.4	PS1 i-band magnitude	mag
e_i_PS1	F7.4	Error on i_PS1	mag
z_PS1	F7.4	PS1 z-band magnitude	mag
e_z_PS1	F7.4	Error on z_PS1	mag
y_PS1	F7.4	PS1 y-band magnitude	mag
e_y_PS1	F7.4	Error on y_PS1	mag
J_2MASS	F6.3	2MASS J-band magnitude	mag
e_J_2MASS	F6.3	Error on J_2MASS	mag
H_2MASS	F6.3	2MASS H-band magnitude	mag
e_H_2MASS	F6.3	Error on H_2MASS	mag
K_2MASS	F6.3	2MASS K-band magnitude	mag
e_K_2MASS	F6.3	Error on K_2MASS	mag
Y_UKIDSS	F6.3	UKIDSS Y-band magnitude	mag
e_Y_UKIDSS	F6.3	Error on Y_UKIDSS	mag
J_UKIDSS	F6.3	UKIDSS J-band magnitude	mag

e_J_UKIDSS	F6.3	Error on J_UKIDSS	mag
H_UKIDSS	F6.3	UKIDSS H-band magnitude	mag
e_H_UKIDSS	F6.3	Error on H_UKIDSS	mag
K_UKIDSS	F6.3	UKIDSS K-band magnitude	mag
e_K_UKIDSS	F6.3	Error on K_UKIDSS	mag
Z_VISTA	F6.3	VISTA surveys (VHS, VIKING) Z-band magnitude	mag
e_Z_VISTA	F6.3	Error on Z_VISTA	mag
Y_VISTA	F6.3	VISTA surveys (VHS, VIKING) Y-band magnitude	mag
e_Y_VISTA	F6.3	Error on Y_VISTA	mag
J_VISTA	F6.3	VISTA surveys (VHS, VIKING) J-band magnitude	mag
e_J_VISTA	F6.3	Error on J_VISTA	mag
H_VISTA	F6.3	VISTA surveys (VHS, VIKING) H-band magnitude	mag
e_H_VISTA	F6.3	Error on H_VISTA	mag
Ks_VISTA	F6.3	VISTA surveys (VHS, VIKING) Ks-band magnitude	mag
e_Ks_VISTA	F6.3	Error on Ks_VISTA	mag
W1	F6.3	WISE W1-band magnitude	mag
e_W1	F6.3	Error on W1	mag
W2	F6.3	WISE W2-band magnitude	mag
e_W2	F6.3	Error on W2	mag
W3	F6.3	WISE W3-band magnitude	mag
e_W3	F6.3	Error on W3	mag
W4	F6.3	WISE W4-band magnitude	mag
e_W4	F6.3	Error on W4	mag

Appendix B: Gaia EDR3 catalogues of hot subluminous star candidates

Table B.1. Catalogue columns

Column	Format	Description	Unit
source_id	I19	Gaia EDR3 source identifier	-
ra	F10.6	Gaia EDR3 Right ascension	deg
dec	F10.6	Gaia EDR3 Declination	deg
l	F10.6	Galactic longitude	deg
b	F10.6	Galactic latitude	deg
parallax	F8.4	Gaia parallax $\bar{\omega}$	mas
parallax_error	F8.4	Error on parallax	mas
abs_g_mag	F8.4	Absolute magnitude in G-band	mag
phot_g_mean_mag	F6.3	Gaia apparent G magnitude	mag
bp_rp	F6.3	Gaia G_{BP} - G_{RP} magnitude	mag
phot_bp_rp_excess_factor_corrected	F6.3	Corrected Gaia G_{BP} - G_{RP} excess factor	-
pmra	F7.3	Gaia proper motion $\mu_\alpha \cos\delta$	mas yr^{-1}
pmra_error	F7.3	Error on pmra	mas yr^{-1}
pmdec	F7.3	Gaia proper motion μ_δ	mas yr^{-1}
pmdec_error	F7.3	Error on pmdec	mas yr^{-1}
pm	F7.3	Gaia proper motion μ	mas yr^{-1}
pm_error	F7.3	Error on proper motion	mas yr^{-1}
ruwe	F7.5	Gaia EDR3 renormalised unit weight error	-
reduced_proper_motion	F7.3	Reduced proper motion H	mag
excess_flux_error	F7.3	Excess flux error	-
parallax_selection_flag	I1	Parallax selection catalogue candidate	-
proper_motion_selection_flag	I1	Proper motion selection catalogue candidate	-